NAVAL POSTGRADUATE SCHOOL

MONTEREY, CALIFORNIA

THESIS

IMPROVING MID-COURSE FLIGHT THROUGH AN APPLICATION OF REAL-TIME OPTIMAL CONTROL

by

Mark R. Roncoroni

December 2017

Thesis Advisor:	Ronald Proulx
Co-Advisor:	Michael Ross

Approved for public release. Distribution is unlimited.

THIS PAGE INTENTIONALLY LEFT BLANK

REPORT DOCUMENTATION PAGE

Form Approved OMB No. 0704–0188

Public reporting burden for this collection of information is estimated to average 1 hour per response, including the time for reviewing instruction, searching existing data sources, gathering and maintaining the data needed, and completing and reviewing the collection of information. Send comments regarding this burden estimate or any other aspect of this collection of information, including suggestions for reducing this burden, to Washington headquarters Services, Directorate for Information Operations and Reports, 1215 Jefferson Davis Highway, Suite 1204, Arlington, VA 22202-4302, and to the Office of Management and Budget, Paperwork Reduction Project (0704-0188) Washington, DC 20503.

1. AGENCY USE ONLY *(Leave blank)*	2. REPORT DATE December 2017	3. REPORT TYPE AND DATES COVERED Master's thesis	
4. TITLE AND SUBTITLE IMPROVING MID-COURSE FLIGHT THROUGH AN APPLICATION OF REAL-TIME OPTIMAL CONTROL		**5. FUNDING NUMBERS**	
6. AUTHOR(S) Mark R. Roncoroni			
7. PERFORMING ORGANIZATION NAME(S) AND ADDRESS(ES) Naval Postgraduate School Monterey, CA 93943-5000		**8. PERFORMING ORGANIZATION REPORT NUMBER**	
9. SPONSORING /MONITORING AGENCY NAME(S) AND ADDRESS(ES) N/A		**10. SPONSORING / MONITORING AGENCY REPORT NUMBER**	

11. SUPPLEMENTARY NOTES The views expressed in this thesis are those of the author and do not reflect the official policy or position of the Department of Defense or the U.S. Government. IRB number ____N/A____.

12a. DISTRIBUTION / AVAILABILITY STATEMENT Approved for public release. Distribution is unlimited.	12b. DISTRIBUTION CODE

13. ABSTRACT (maximum 200 words)

Improving the performance of a missile weapon system is a consistently sought-after goal. A common method to accomplish this is to use a more efficient physical design. This thesis explores a proof-of-concept solution to the problem by improving guidance laws through the application of optimal control theory to enhance its performance.

A modified 3-degrees of freedom (3-DOF) model of a tactical missile was developed using common methods for estimating aerodynamic properties. Once the 3-DOF model problem was properly formulated with relevant cost functions and boundary conditions, Pontryagin's principle on optimal control was then applied to develop the necessary Boundary Value Problem that can be used to find the optimal guidance solution. The derived solution was then applied to another 3-DOF model with an improved fidelity of aerodynamic properties to show the potential of real-time optimal control (RTOC).

The resulting miss distance was used to assess update rate requirements for real-time, optimal mid-course guidance. Finally, the conservation of kinetic energy over the course of flight was used to compare RTOC performance to that of traditional proportional navigation control laws and demonstrate the potential of RTOC.

14. SUBJECT TERMS Optimal Guidance, Real-Time Optimal Control, DIDO, Missile DATCOM, High-Fidelity modeling, Low-Fidelity Modeling, Proportional Navigation	15. NUMBER OF PAGES 95
	16. PRICE CODE

17. SECURITY CLASSIFICATION OF REPORT Unclassified	18. SECURITY CLASSIFICATION OF THIS PAGE Unclassified	19. SECURITY CLASSIFICATION OF ABSTRACT Unclassified	20. LIMITATION OF ABSTRACT UU

i

THIS PAGE INTENTIONALLY LEFT BLANK

**IMPROVING MID-COURSE FLIGHT THROUGH AN APPLICATION OF
REAL-TIME OPTIMAL CONTROL**

Mark R. Roncoroni
Lieutenant, United States Navy
B.S., United States Naval Academy, 2010

Submitted in partial fulfillment of the
requirements for the degree of

MASTER OF SCIENCE IN ASTRONAUTICAL ENGINEERING

from the

**NAVAL POSTGRADUATE SCHOOL
December 2017**

Approved by: Ronald Proulx
                      Thesis Advisor

                      Michael Ross
                      Co-Advisor

                      Garth V. Hobson
                      Chair, Department of Mechanical and Aerospace Engineering

THIS PAGE INTENTIONALLY LEFT BLANK

ABSTRACT

Improving the performance of a missile weapon system is a consistently sought-after goal. A common method to accomplish this is to use a more efficient physical design. This thesis explores a proof-of-concept solution to the problem by improving guidance laws through the application of optimal control theory to enhance its performance.

A modified 3-degrees of freedom (3-DOF) model of a tactical missile was developed using common methods for estimating aerodynamic properties. Once the 3-DOF model problem was properly formulated with relevant cost functions and boundary conditions, Pontryagin's principle on optimal control was then applied to develop the necessary Boundary Value Problem that can be used to find the optimal guidance solution. The derived solution was then applied to another 3-DOF model with an improved fidelity of aerodynamic properties to show the potential of real-time optimal control (RTOC).

The resulting miss distance was used to assess update rate requirements for real-time, optimal mid-course guidance. Finally, the conservation of kinetic energy over the course of flight was used to compare RTOC performance to that of traditional proportional navigation control laws and demonstrate the potential of RTOC.

THIS PAGE INTENTIONALLY LEFT BLANK

TABLE OF CONTENTS

LIST OF FIGURES

LIST OF TABLES

THIS PAGE INTENTIONALLY LEFT BLANK

LIST OF ACRONYMS AND ABBREVIATIONS

3-DOF	three degrees of freedom
6-DOF	six degrees of freedom
BVP	boundary value problem
CA	axial coefficient
c.g.	center of gravity
Cl	rolling moment coefficient
c.m.	center of mass
Cm	moment coefficient
CN	normal coefficient
Cn	yawing moment coefficient
CY	side-force coefficient
DCM	direction cosine matrix
ECEF	Earth-centered, Earth-fixed
ECI	Earth-centered inertial
KKT	Karush-Kuhn-Tucker
MOI	moments of inertia
RTOC	real-time optimal control

THIS PAGE INTENTIONALLY LEFT BLANK

ACKNOWLEDGMENTS

Above all, I would like to thank my wife, Anne Jefferson, for all her love and support during my time at the Naval Postgraduate School. Despite our being separated by your work in the Guard, you have always been there for me when times became difficult. Thank you for everything. I love you more than anything.

Second, I would like to thank my advisor, Dr. Ronald Proulx, for his long-distance support from Massachusetts. Your experience was crucial in keeping the objective in sight and debugging my system during less than optimal times.

To Dr. Mike Ross and Dr. Mark Karpenko, thank you for your time, effort, and enthusiasm on the subject. Your classes over the years helped fuel the passion I have for control theory from my undergraduate years. Thank you.

Finally, I would like to thank all my instructors. The knowledge I have obtained here at NPS has fed my curiosity and desire to learn more. Thank you all.

THIS PAGE INTENTIONALLY LEFT BLANK

I.   INTRODUCTION

The history of missile guidance can be traced back to World War II with the Germans conducting research into proportional navigation to aide in engaging moving targets [1]. However, it was not until after the end of the war when the post-war scientists migrated to the Unites States that the research was complete. This resulted in the development of the Lark weapon system, and the first successful intercept by a missile on December 2, 1950 [1].

Since the initial Lark's success, a significant amount of effort has been put into further developing missile guidance, focused on improving how the proportional guidance was implemented. Some of these methods include utilizing gain scheduling which takes a pre-determined series of gains for different system parameters [2], while other methods use the power of machine learning to teach the system to be able to calculate the necessary gains during flight [2]. Further still, Linear Quadratic optimal control is used to derive the optimal impact angle, but still employs a form of proportional feedback [2].

This thesis will explore another method for solving the missile guidance problem that employs a form of feedback loop other than proportional gain. Unlike the other methods, Pontryagin's principle for optimal control does not require any sort of feedback to generate the control input. Instead, it produces the control for the entire time of maneuver that is needed to minimize the specified cost function. This is, however, not without shortcomings. If the dynamics used to solve the optimal control problem are not accurate, or less complex than the actual conditions then the calculated solution may not provide a workable solution. This is where real-time optimal control (RTOC) can be used to create a "feedback" loop and solves the model uncertainty issue by periodically solving the optimal control problem throughout the flight of the missile. This thesis explores applying RTOC to a hypothetical missile. The optimal control is developed using estimated aerodynamic coefficients and is simulated with more robust coefficients. The process is then finalized by comparing the results versus a traditional proportional navigation control law.

Chapter II develops the mathematical model used for solving the optimal control problem. First the ideas of reference frames and orientations are introduced and applied to the problem. After establishing the required rotations, the dynamics are then introduced with much help from Kevin Bolino's dissertation [3] on "High-Fidelity Real-Time Trajectory Optimization for Reusable Launch Vehicles." The chapter is finished by introducing a non-standard 3-degree of freedom (3-DOF) model derived from Bolino's 6-degree of freedom (6-DOF) model.

Chapter III takes on the challenge of estimating the aerodynamics coefficients of a generic missile. An AIM-120 missile is used as a reference body and the physical characteristics are obtained from open source references and extrapolated to fill in the data gaps. Missile DATCOM is then introduced, which is used with the physical characteristics to estimate what the coefficients might be. The concept of high-fidelity vs. low-fidelity models is then introduced and how they will be applied to the problem at hand.

Chapter IV introduces the optimal control problem. First, Pontryagin's principle of optimal control is introduced and its applicability to our problem described. The principle is then applied, step by step, to the maximum distance problem. The associated boundary value problem (BVP) is developed. Finally, the program DIDO is introduced which is used to solve the resulting BVP after scaling and balancing the problem.

Chapter V introduces a basic implementation of the proportional navigation by defining the calculations used to develop the control law. The generated acceleration from the proportional navigation control law is then converted to the controls used by the model.

Chapter VI finalizes the entire process by simulating the results. Solutions derived by DIDO are checked through a series of verifications and validations (V&V). Expected co-states and Hamiltonian values are verified and the same model used to compute the solution is propagated. Once the V&V has been conducted, the control is then fed into the high-fidelity model that implements a real-time optimal control feedback loop. Some conclusions, research and suggestions for future work are given in Chapter VII.

II.   DYNAMIC MODELS

Before work on any problem can be done, the problem must first be defined. This chapter intends to do that. The chapter begins with defining the reference frames and coordinates that will be employed by the model, and the rotations between them. With the rotations established the 6- DOF dynamics are then introduced. The 6-DOF model is then reduced to a non-standard 3-DOF model that will be used to develop the optimal control for this thesis and simulations using MathWorks' Simulink.

A.   REFERENCE FRAMES

The first step in developing an aerodynamic model, or any model for that matter, is to define the reference frames and coordinate systems that will be used. In the case of a generic missile, a body and an inertial frame are needed to describe the motion of the missile.

First, the body frame is attached to the center of gravity (*c.g.*) of the missile's body, which is later calculated in Chapter III, Section A. With the frame attached to the *c.g.* the coordinate system is defined by using the right-hand rule, aligning the *X*-axis along the centerline of the missile, pointing from the *c.g.* towards the nose of the missile. Because missiles are typically symmetric about their centerline, the direction of the *Z* and *Y*-axis can be arbitrary. However, to ensure that when the moments of inertia, MOI, matrix will be diagonal in the body frame, the *Z*-axis is chosen to be in line with the fin and wing groups 1 and 3, pointing from the *c.g.* to 3, and the *Y*-axis in line with the fin and wing groups 2 and 4, pointing from the *c.g.* to 2. Figure 1 provides a visual of the body frame and coordinates.
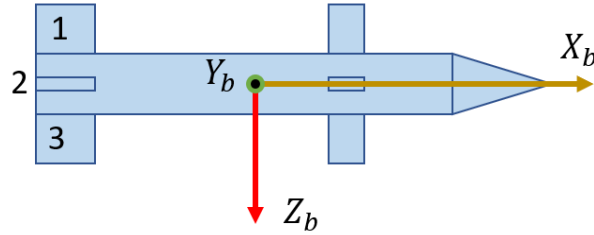
Figure 1. *X-Z* Plane View of Body Frame Attached to Missile Body

With the body frame and coordinates defined, the next frame to define is the inertial. The inertial frame and coordinates are important because they are used to describe the motion of the body in physical space and provide a context to the observed motion. An inertial frame can be placed anywhere in space, but it needs to make sense in the context of the motion and what we as observers care about. For example, although choosing the center of the Sun for our inertial frame and coordinates is allowed, it is unreasonable in the context of a short-range missile. We simply do not care how far our missile travels in relation to the Sun's core. A more reasonable inertia frame would need to be located somewhere on the Earth.

Because the missile will be traveling a small distance over the surface of the Earth, in relation to the Earth itself, the Local-Tangent frame makes the most sense. In addition to using the Local-Tangent frame, a flat-Earth approximation will also be used to further simplify the problem. The positive Z direction will perpendicular to the tangent-plane and pointed away from the Earth's surface, while the X-Y plane will be along the tangent-plane, as shown in Figure 2.

4
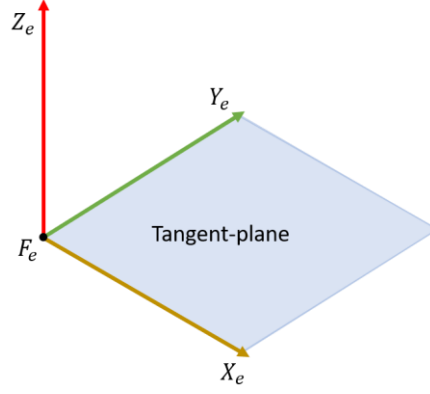
Figure 2. Local-Tangent Inertial Frame and Coordinates

B.   ORIENTATION AND ROTATION

All the motions of the missile occur in the inertial coordinate system; however, it can be easier to calculate the forces and moments acting on the missile in the body frame first and then translate the results into the inertial coordinate system. To do this, the orientation of the body coordinates need to be described in relation to the inertial coordinates and vice versa. One method for doing this is to use a direction cosine matrix (DCM). The DCM can be used to describe the expression of one coordinate system with respect to another or the orientation of an object within a single coordinate system.

A DCM can be developed by considering a sequence of rotations about the axes $[X,Y,Z]$ with $[\varphi,\theta,\psi]$ being the amount of rotation for each axis [3].

$$R_x = \begin{pmatrix} 1 & 0 & 0 \\ 0 & \cos\varphi & \sin\varphi \\ 0 & -\sin\varphi & \cos\varphi \end{pmatrix}, \qquad \text{(eq. 1)}$$

$$R_y = \begin{pmatrix} \cos\theta & 0 & -\sin\theta \\ 0 & 1 & 0 \\ \sin\theta & 0 & \cos\theta \end{pmatrix}, \qquad \text{(eq. 2)}$$

5

$$R_z = \begin{pmatrix} \cos\psi & \sin\psi & 0 \\ -\sin\psi & \cos\psi & 0 \\ 0 & 0 & 1 \end{pmatrix}. \qquad \text{(eq. 3)}$$

Each rotation that is made is based on the new orientation that the previous resulted in. For example, if a set of coordinates are first rotated about the X-axis, then the Z-axis, then the first rotation about the X-axis would look like

$$\begin{bmatrix} X_2 \\ Y_2 \\ Z_2 \end{bmatrix} = R_x \begin{bmatrix} X_1 \\ Y_1 \\ Z_1 \end{bmatrix}. \qquad \text{(eq. 4)}$$

The second rotation about the Z-axis would then be

$$\begin{bmatrix} X_3 \\ Y_3 \\ Z_3 \end{bmatrix} = R_z \begin{bmatrix} X_2 \\ Y_2 \\ Z_2 \end{bmatrix}. \qquad \text{(eq. 5)}$$

Substituting (eq. 4) into (eq. 5) shows that a new DCM can be made by multiplying the two rotations together,

$$\begin{bmatrix} X_3 \\ Y_3 \\ Z_3 \end{bmatrix} = R_z R_x \begin{bmatrix} X_1 \\ Y_1 \\ Z_1 \end{bmatrix} = R_{zx} \begin{bmatrix} X_1 \\ Y_1 \\ Z_1 \end{bmatrix}. \qquad \text{(eq. 6)}$$

Using this information, one DCM can be generated by using the standard order of rotations of R_z, R_y, then R_x,

$$R_o^{\,i} = R_x R_y R_z = \begin{pmatrix} \cos\theta\cos\psi & \cos\theta\sin\psi & -\sin\theta \\ \sin\varphi\sin\theta\cos\psi - \cos\varphi\sin\psi & \sin\varphi\sin\theta\sin\psi + \cos\varphi\cos\psi & \sin\varphi\cos\theta \\ \cos\varphi\sin\theta\cos\psi + \sin\varphi\sin\psi & \cos\varphi\sin\theta\sin\psi - \sin\varphi\cos\psi & \cos\varphi\cos\theta \end{pmatrix}, \text{(eq. 7)}$$

where i is the initial coordinate system and o is the final coordinate system.

6

Now that a means of expressing one frame in another, an initial orientation between the body and inertial coordinates needs to be established. X_b will be in the positive direction of X_e and Z_b will point in the negative direction of Z_e. Figure 3 demonstrates this orientation.
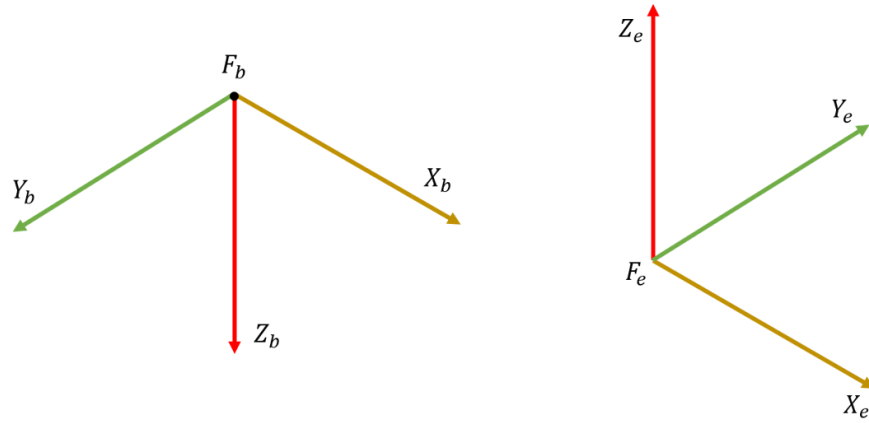
Figure 3. Body (Left) and Inertially (Right) Frame

Figure 3 also shows that only a rotation about X_b, $\varphi = \pi$, is needed to complete the translation, meaning $\theta = \psi = 0$

$$R_e^b = \begin{pmatrix} 1 & 0 & 0 \\ 0 & -1 & 0 \\ 0 & 0 & -1 \end{pmatrix}, \tag{eq. 8}$$

where b represents the body coordinates and e represents the inertial coordinates.

If the missile was only translating along the axes, equation (eq. 8) would be enough to express the body in the inertial frame. However, because the missile can also rotate, due to aerodynamic drag, within the inertial frame, equation (eq. 8) becomes an intermediate step and is relabeled as

7

$$R_o^b = \begin{pmatrix} 1 & 0 & 0 \\ 0 & -1 & 0 \\ 0 & 0 & -1 \end{pmatrix}.$$ (eq. 9)

where o is the intermediate orientation. The next rotation then takes the intermediate orientation and expresses that in the inertial frame. This by done by again using equation (eq. 7).

$$R_e^o = \begin{pmatrix} \cos\theta\cos\psi & \cos\theta\sin\psi & -\sin\theta \\ \sin\varphi\sin\theta\cos\psi - \cos\varphi\sin\psi & \sin\varphi\sin\theta\sin\psi + \cos\varphi\cos\psi & \sin\varphi\cos\theta \\ \cos\varphi\sin\theta\cos\psi + \sin\varphi\sin\psi & \cos\varphi\sin\theta\sin\psi - \sin\varphi\cos\psi & \cos\varphi\cos\theta \end{pmatrix}.$$ (eq. 10)

To obtain the complete DCM the two rotations are combined using matrix multiplication with body rotated to the intermediate orientation first, and then to the inertial frame.

$$R_e^b = R_e^o R_o^b = \begin{pmatrix} \cos\theta\cos\psi & -\cos\theta\sin\psi & \sin\theta \\ \sin\varphi\sin\theta\cos\psi - \cos\varphi\sin\psi & -\sin\varphi\sin\theta\sin\psi - \cos\varphi\cos\psi & -\sin\varphi\cos\theta \\ \cos\varphi\sin\theta\cos\psi + \sin\varphi\sin\psi & -\cos\varphi\sin\theta\sin\psi + \sin\varphi\cos\psi & -\cos\varphi\cos\theta \end{pmatrix}.$$ (eq. 11)

The DCM to express the body frame in the inertial frame is now available. Reversing the process then allows the inertial frame to be then expressed in the body frame [3],

$$R_b^e = \begin{pmatrix} \cos\theta\cos\psi & \sin\varphi\sin\theta\cos\psi - \cos\varphi\sin\psi & \cos\varphi\sin\theta\cos\psi + \sin\varphi\sin\psi \\ -\cos\theta\sin\psi & -\sin\varphi\sin\theta\sin\psi - \cos\varphi\cos\psi & -\cos\varphi\sin\theta\sin\psi + \sin\varphi\cos\psi \\ \sin\theta & -\sin\varphi\cos\theta & -\cos\varphi\cos\theta \end{pmatrix}.$$ (eq. 12)

C.   SIX DEGREES OF FREEDOM MODEL

When developing the six degree of freedom (6-DOF) model the important positions, velocities, and accelerations need to be defined in their respected frames. the velocities of the body, in the body coordinates, are represented by $[u, v, w]$,

8

$$\begin{bmatrix} \dot{X} \\ \dot{Y} \\ \dot{Z} \end{bmatrix}^{b} = \begin{bmatrix} u \\ v \\ w \end{bmatrix}. \tag{eq. 13}$$

The angular velocities of the body, in the body coordinates, are represented by $[p,q,r]$,

$$\begin{bmatrix} \omega_{x} \\ \omega_{y} \\ \omega_{z} \end{bmatrix}^{b} = \begin{bmatrix} p \\ q \\ r \end{bmatrix}. \tag{eq. 14}$$

The position of the missile, in the inertial frame, is represented by $[X_{e},Y_{e},Z_{e}]$,

$$\begin{bmatrix} X \\ Y \\ Z \end{bmatrix}^{e} = \begin{bmatrix} X_{e} \\ Y_{e} \\ Z_{e} \end{bmatrix}. \tag{eq. 15}$$

The rotation of the missile, in the inertial frame, is represented by $[\psi,\theta,\varphi]$,

$$\begin{bmatrix} \psi \\ \theta \\ \varphi \end{bmatrix}^{e} = \begin{bmatrix} \psi \\ \theta \\ \varphi \end{bmatrix}. \tag{eq. 16}$$

1.   Forces

As mentioned earlier, it is simpler to calculate the forces and moments in the body frame and then convert the resulting velocities from the body to the internal frame [3]. With this in mind, the forces acting on the body can be summarized as

$$\begin{bmatrix} F_{X} \\ F_{Y} \\ F_{Z} \end{bmatrix}^{b} = \begin{bmatrix} \bar{q}S_{ref}CA + F_{g_{X}} + F_{T} \\ \bar{q}S_{ref}CY + F_{g_{Y}} \\ \bar{q}S_{ref}CN + F_{g_{Z}} \end{bmatrix}, \tag{eq. 17}$$

where $\bar{q}$ is known as the dynamic pressure, S_{ref} is the reference area of the body, $[CA,CY,CN]^{T}$ are the axial coefficient of drag, side-force coefficient of drag, and normal coefficient of drag. Vector $[F_{gx},F_{gy},F_{gz}]^{T}$ represents the force of gravity in the

9

body frame, and F_T is the thrust generated by the missile motor. Because we will be focusing on the midcourse phase of flight, which is starts when the motor burns out, $F_T = 0$.

The dynamic pressure is obtained by [3]

$$\bar{q} = \frac{1}{2}\rho(Z_e)V^2. \tag{eq. 18}$$

where ρ is the air density, as defined by the barometric function [4],

$$\rho = 1.225e^{-0.0001184Z_e}. \tag{eq. 19}$$

and V is

$$V = \begin{bmatrix} u + W_X \\ v + W_Y \\ w + W_Z \end{bmatrix}^b, \tag{eq. 20}$$

where $[W_X, W_Y, W_Z]^T$ are the wind velocities in F_b. For this thesis, it is assumed there is no wind, $[W_X, W_Y, W_Z]^T = 0$.

Using equation (eq. 12) the forces of gravity in the body frame can be determined.

$$\begin{bmatrix} F_{gx} \\ F_{gy} \\ F_{gz} \end{bmatrix}^b = R_b^e \begin{bmatrix} 0 \\ 0 \\ -mg \end{bmatrix}^e = \begin{bmatrix} -mg(\cos\varphi\cos\psi\sin\theta + \sin\varphi\sin\psi) \\ -mg(-\cos\varphi\sin\psi\sin\theta + \cos\psi\sin\varphi) \\ -mg(-\cos\varphi\cos\theta) \end{bmatrix}, \tag{eq. 21}$$

where m is the mass of the missile and g is the gravitational acceleration. Force can also be represented as the time derivative of linear momentum. By representing force as the time derivative of linear momentum the influence of the angular rates on the force can be seen through the cross product between of the angular rates and the momentum of the missile [3].

$$F = \frac{d(mV)}{dt} = \frac{\delta(mV)}{\delta t} + (\omega + \omega_e) \times (mV), \tag{eq. 22}$$

where $\omega = [p, q, r]^T$ and $\omega_e = [p_e, q_e, r_e]^T$. Because this thesis is using the flat earth approximation, $\omega_e = 0$. Equation (eq. 22) becomes

$$\begin{bmatrix} F_X \\ F_Y \\ F_Z \end{bmatrix}^b = \begin{bmatrix} m(\dot{u} + qw - rv) \\ m(\dot{v} + ru - pw) \\ m(\dot{w} + pv - qw) \end{bmatrix}. \qquad \text{(eq. 23)}$$

It is now possible to equate equations (eq. 17) and (eq. 23),

$$\begin{bmatrix} \bar{q}S_{ref}CA + F_{gx} \\ \bar{q}S_{ref}CY + F_{gy} \\ \bar{q}S_{ref}CN + F_{gz} \end{bmatrix} = \begin{bmatrix} m(\dot{u} + qw - rv) \\ m(\dot{v} + ru - pw) \\ m(\dot{w} + pv - qw) \end{bmatrix}, \qquad \text{(eq. 24)}$$

and then solve for $\dot{V}$,

$$\begin{bmatrix} \dot{u} \\ \dot{v} \\ \dot{w} \end{bmatrix} = \begin{bmatrix} \dfrac{\bar{q}S_{ref}CA}{m} - g(\sin\varphi\sin\psi + \cos\varphi\cos\psi\sin\theta) - qw + rv \\ \dfrac{\bar{q}S_{ref}CY}{m} - g(\cos\psi\sin\varphi - \cos\varphi\sin\psi\sin\theta) - ru - pw \\ \dfrac{\bar{q}S_{ref}CN}{m} + g\cos\varphi\cos\theta - pv + qw \end{bmatrix}. \qquad \text{(eq. 25)}$$

Equation (eq. 25) now provides the accelerations of the body expressed in the body coordinates.

2. Moments

With the forces obtained, the next step is to find the moments acting on the body expressed in the body coordinates. Because the body does not have any irregular mass distribution, is short in length, and total flight time relatively short, any gravitational field effects can be assumed to be negligible, meaning that only aerodynamics forces are considered in the moments acting on the body [3].

$$\begin{bmatrix} M_X \\ M_Y \\ M_Z \end{bmatrix}^b = \begin{bmatrix} \bar{q}S_{ref}Cl \\ \bar{q}S_{ref}Cm \\ \bar{q}S_{ref}Cn \end{bmatrix}, \tag{eq. 26}$$

where $[Cl, Cm, Cn]^T$ are the rolling moment coefficient, pitching moment coefficient, and the yawing moment coefficient.

Similar to the forces, the moments can be represented as the time derivative of angular momentum, h [3].

$$M = \frac{dh}{dt} = \frac{\delta \vec{h}}{\delta t} + \omega \times \vec{h}, \tag{eq. 27}$$

where h is the matrix-vector product of the moments of inertia and the angular velocities,

$$h = \begin{bmatrix} I_{XX} & -I_{XY} & -I_{XZ} \\ -I_{YX} & I_{YY} & -I_{YZ} \\ -I_{ZX} & -I_{ZY} & I_{ZZ} \end{bmatrix} \begin{bmatrix} p \\ q \\ r \end{bmatrix}. \tag{eq. 28}$$

If the origin of the body coordinates is chosen to be at the *c.g.* of the missile and the axes are chosen to be so that they align with the principle moments of inertia, which is easily done with a missile, then h becomes [3]

$$h = \begin{bmatrix} I_{XX} & 0 & 0 \\ 0 & I_{YY} & 0 \\ 0 & 0 & I_{ZZ} \end{bmatrix} \begin{bmatrix} p \\ q \\ r \end{bmatrix} = \begin{bmatrix} I_{XX}p \\ I_{YY}q \\ I_{ZZ}r \end{bmatrix}. \tag{eq. 29}$$

The moments expressed in the body frame are then

$$\begin{bmatrix} M_X \\ M_Y \\ M_Z \end{bmatrix}^b = \begin{bmatrix} I_{XX}\dot{p} + (I_{ZZ} - I_{YY})qr \\ I_{YY}\dot{q} + (I_{XX} - I_{ZZ})pr \\ I_{ZZ}\dot{r} + (I_{YY} - I_{XX})pq \end{bmatrix}, \tag{eq. 30}$$

and combining equations (eq. 26) and (eq. 30), and solving for $[\dot{p}, \dot{q}, \dot{r}]$ gives

12

$$\begin{bmatrix} \dot{p} \\ \dot{q} \\ \dot{r} \end{bmatrix} = \begin{bmatrix} \dfrac{\bar{q}S_{ref}Cl - (I_{zz} - I_{yy})qr}{I_{xx}} \\ \dfrac{\bar{q}S_{ref}Cm - (I_{xx} - I_{zz})pr}{I_{yy}} \\ \dfrac{\bar{q}S_{ref}Cn - (I_{yy} - I_{xx})pq}{I_{zz}} \end{bmatrix}. \qquad \text{(eq. 31)}$$

3. Inertial Motion

Now that the linear and rotational accelerations in the body have been found, the next step is to determine how the linear and rotational velocities of the body relate to motion in the inertial frame. This is easily done by applying equation (eq. 11) to the velocities and angular rates of the body. The velocities in the inertial frame will be

$$\begin{bmatrix} \dot{X}_e \\ \dot{Y}_e \\ \dot{Z}_e \end{bmatrix}^e = \begin{bmatrix} u\cos\psi\cos\theta - v\cos\theta\sin\psi + w\sin\theta \\ -u(\cos\varphi\sin\psi - \cos\psi\sin\varphi\sin\theta) - v(\cos\varphi\cos\psi + \sin\varphi\sin\psi\sin\theta) - w\cos\theta\sin\varphi \\ u(\sin\varphi\sin\psi + \cos\varphi\cos\psi\sin\theta) + v(\cos\psi\sin\varphi - \cos\varphi\sin\psi\sin\theta) - w\cos\varphi\cos\theta \end{bmatrix} \text{(eq. 32)}$$

and the angular rates will be

$$\begin{bmatrix} \dot{\psi} \\ \dot{\theta} \\ \dot{\varphi} \end{bmatrix} = \begin{bmatrix} p\cos\psi\cos\theta - q\cos\theta\sin\psi + r\sin\theta \\ -p(\cos\varphi\sin\psi - \cos\psi\sin\varphi\sin\theta) - q(\cos\varphi\cos\psi + \sin\varphi\sin\psi\sin\theta) - r\cos\theta\sin\varphi \\ p(\sin\varphi\sin\psi + \cos\varphi\cos\psi\sin\theta) + q(\cos\psi\sin\varphi - \cos\varphi\sin\psi\sin\theta) - r\cos\varphi\cos\theta \end{bmatrix}. \text{(eq. 33)}$$

4. Putting the 6-DOF Model Together

Now that the form of each of the components of the 6-DOF model have been determined, the 6-DOF model of the missile can be assembled into

13

$$\dot{u} = \frac{\overline{q}S_{ref}CA}{m} - g(\sin\varphi\sin\psi + \cos\varphi\cos\psi\sin\theta) - qw + rv$$

$$\dot{v} = \frac{\overline{q}S_{ref}CY}{m} - g(\cos\psi\sin\varphi - \cos\varphi\sin\psi\sin\theta) - ru - pw$$

$$\dot{w} = \frac{\overline{q}S_{ref}CN}{m} + g\cos\varphi\cos\theta - pv + qw$$

$$\dot{p} = \frac{\overline{q}S_{ref}Cl - (I_{zz} - I_{yy})qr}{I_{xx}}$$

$$\dot{q} = \frac{\overline{q}S_{ref}Cm - (I_{xx} - I_{zz})pr}{I_{yy}}$$

$$\dot{r} = \frac{\overline{q}S_{ref}Cn - (I_{yy} - I_{xx})pq}{I_{zz}}$$

$$\dot{X}_e = u\cos\psi\cos\theta - v\cos\theta\sin\psi + w\sin\theta$$

$$\dot{Y}_e = -u(\cos\varphi\sin\psi - \cos\psi\sin\varphi\sin\theta) - v(\cos\varphi\cos\psi + \sin\varphi\sin\psi\sin\theta) - w\cos\theta\sin$$

$$\dot{Z}_e = u(\sin\varphi\sin\psi + \cos\varphi\cos\psi\sin\theta) + v(\cos\psi\sin\varphi - \cos\varphi\sin\psi\sin\theta) - w\cos\varphi\cos\theta$$

$$\dot{\psi} = p\cos\psi\cos\theta - q\cos\theta\sin\psi + r\sin\theta$$

$$\dot{\theta} = -p(\cos\varphi\sin\psi - \cos\psi\sin\varphi\sin\theta) - q(\cos\varphi\cos\psi + \sin\varphi\sin\psi\sin\theta) - r\cos\theta\sin\varphi$$

$$\dot{\varphi} = p(\sin\varphi\sin\psi + \cos\varphi\cos\psi\sin\theta) + q(\cos\psi\sin\varphi - \cos\varphi\sin\psi\sin\theta) - r\cos\varphi\cos\theta$$

$$\overline{q} = \frac{1}{2}\rho(Z_e)|V|^2 \quad \rho = 1.225e^{-0.0001184Z_e}$$

. (eq. 34)

D. THREE DEGREES OF FREEDOM MODEL

Typically, when talking about a three degree of freedom (3-DOF) model, this implies that only lateral translations, $[u, v, w]$, will be considered. For our purposes, a non-standard 3-DOF will be used, $[u, q, w]$. The non-standard model was used because it was assumed that the motion of the missile when tracking a stationary target would be within a single plane and did not wish to reduce the model to 2-DOF. To obtain the 3-DOF equations of motion, the "unused" motion, $[p, v, r]$, are set to zero and then applied to 6-DOF equations of motion. The resulting equations are then used for the 3-DOF model. The results are summarized as

14

$$\dot{u} = \frac{\bar{q}S_{ref}CA}{m} - qw - g\sin\theta$$

$$\dot{q} = \frac{\bar{q}S_{ref}CM}{I_{yy}}$$

$$\dot{w} = \frac{\bar{q}S_{ref}CN}{m} + qw + g\cos\theta$$

$$\dot{X}_e = u\cos\theta + w\sin\theta$$

$$\dot{\theta} = -q$$

$$\dot{Z}_e = u\sin\theta - w\cos\theta$$

$$\bar{q} = \frac{1}{2}\rho(Z_e)|V|^2 \quad \rho = 1.225e^{-0.0001184Z_e}$$

(eq. 35)

E.   SUMMARY

This chapter covered the development of the dynamics that are used to simulate the model. The concepts of frames and coordinates we addressed and then applied to the missile body and an inertial reference. Rotations we then developed to be able to express motion in one set of coordinates by first building the standard 6-DOF model, and then simplifying it to a non-standard 3-DOF model.

THIS PAGE INTENTIONALLY LEFT BLANK

III.   AERODYNAMIC COEFFICIENTS

To model the dynamics of a missile as accurately as possible the aerodynamic coefficients must be determined. Aerodynamic coefficients can be very difficult to determine because they depend on many factors such as the shape of body, the material of the body, the air density (ρ), the angle of attack (α), sideslip angle (β), and air speed. Because of all these factors, the coefficients are not constant throughout flight. To this day, the best method for determining the aerodynamic coefficients would be to place an exact mockup of the body into a wind tunnel and test all different configurations. While this method is the most accurate, it can be cost and time prohibitive when testing various design choices. Another issue with this method, for the purpose of this work, is the sensitive nature of the data.

Some references, such as Zarchan [5] provide a means to calculate an estimate of the normal coefficient values, but are only good for a relatively small α due to the non-linear nature of the coefficients. This method can be useful when calculating the optimal solution, but a more accurate method is needed for real world comparison and simulation. Fortunately, there exists another method. The U.S. Air Force Research Laboratory developed a program known as Missile DATCOM. The purpose of Missile DATCOM is to provide a means of calculating the aerodynamic coefficients with an accuracy suitable for preliminary design [6]**.**

A.   PHYSICAL CHARACTERISTICS

Missile DATCOM can take many factors into account when calculating the aerodynamic coefficients of a body. It is possible to input the shape and location of the different fin sets of a missile, the nose shape and length, the skin material of the missile, the altitude of flight, the Mach range to be used, angle of attack, side slip angle, and much more. To use Missile DATCOM to calculate the aerodynamics coefficients, the first step was to determine the physical parameters of a generic missile.

The AIM-120C missile was chosen to act as a reference for building the generic missile used in the simulation. Using open source information [7], it is possible to come

up with a good starting point for determining the dimensions of the missile. Using the information in Table 1, a sample image of an AIM-120, as seen in Figure 4, and pixel analysis using the image analyzing software ENVI [8], a rough blueprint of the missile was constructed (see Figure 5).

Table 1.   AIM-120C Characteristics. Adapted from [7].

Length	3.66 m
Diameter	17.8 cm
Wingspan	53.3 cm
Finspan	63.5 cm
Weight	157 kg
Max Speed	Mach 4
Max Range	105 km
Propulsion	Hercules/Aerojet Solid-fueled rocket
Warhead	18 kg WDU-41

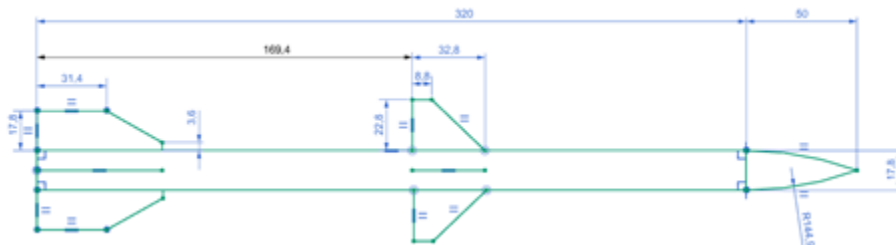Figure 4. AIM-120C. Source: [7].

Figure 5. Estimated Dimensions of AIM-120 (Dimensions in cm)

18

With the physical dimensions of the missile obtained, the next piece of information needed for Missile DATCOM was the location of the center of gravity (*c.g.*). First the missile in Figure 5 is broken down in the following components:

- Motor
- Warhead
- Electronics
- Cone
- Fins
- Wings

While the location of the wings and fins were already determined earlier, Figure 6 was used as a way to estimate the location and size of the remaining components. Figure 7 shows how these components fit into our design.
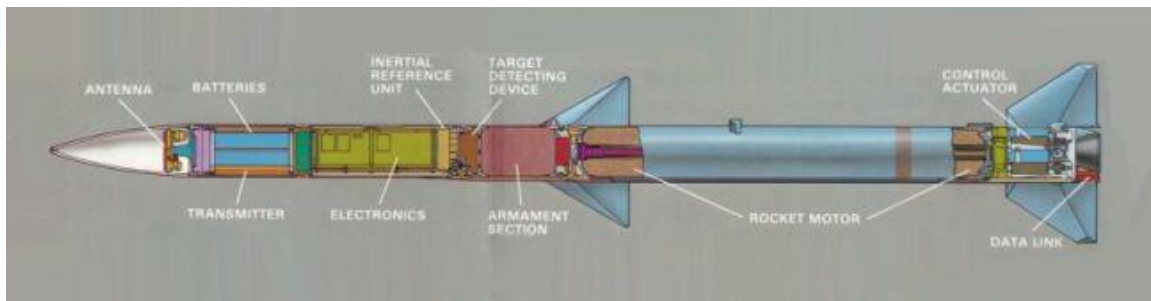
Figure 6. Reference AIM-120 Internal Components. Source: [8].
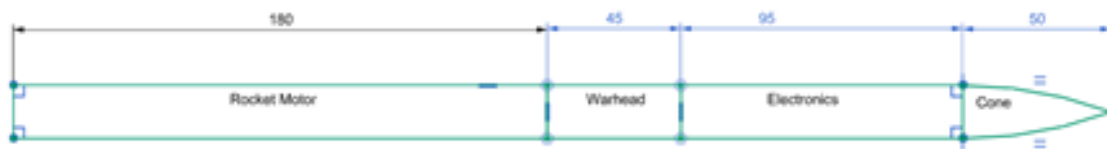
Figure 7. Estimated Layout of AIM-120 Internal Components

With the components identified and their locations determined, each individual *c.g.* needed to be determined. When determining the body components *c.g.*, two assumptions were made. First, the components have uniform density, and second, the mass included the skin of the body surrounding the component. First, we know that the missile has a total weight of 157 *kg* [7]. It is also known that the warhead has a mass of

18 *kg* [8]. If the fins and wings are assumed to have a uniform thickness of 6 mm, their volume can be calculated. It is assumed that they are made of solid titanium, which has a density of 4.5 g/cm^3, the fins and wings have a mass of combined mass of 11 *kg* and 5 *kg* respectively. This leaves *123* kg remaining for the motor, electronics, and cone.

When determining the mass of the motor, two different mass totals can be considered: wet mass and dry mass. To determine the mass of the motor a report by Tyrell et al[9]. was consulted. The report first states that open source information on the AIM-120 missile shows that the motor has a total mass of 75 kg [9]. The report then goes on to use CAD to model the motor and determine the amount of fuel within the motor, which they estimated to be 50 kg [9]. This suggests that the wet mass of the missile is 157 kg and the dry mass is 107 kg. In addition, the report also estimates that the thrust of the motor to be around 16772 N [9].

At this point it is known that the electronics and cone have a combined mass of 48 kg and is was decided to combine the two components into one. Table 2 summarizes the mass distribution.

Table 2.   Estimated Mass Distribution of AIM-120C

Component	Mass
Electronics and Cone	48 kg
Warhead	18 kg
Fins	11 kg
Wings	5 kg
Motor	Wet: 75 kg Dry: 25 kg
Total	Wet 157 kg Dry: 107 kg

With the mass distribution known, the *c.g.* can be calculated. In addition, the moments of inertia (MOI) can also be determined, which will be useful later when simulating the missile dynamics. First the *c.g.* is calculated. Because the axes were chosen to be on the principle axes of inertia, and the missile is symmetric about the *X*-axis, the *c.g.* of the missile is located somewhere along the *X*-axis. Each component was then assumed to have a uniform density and therefore could be estimated as point-masses,

$$c.g. = \frac{\sum_n c.g._{n} m_n}{m_t} . \qquad \text{(eq. 36)}$$

Where $c.g._{n}$ is the center of gravity of each of the components, measured from the tail of the missile, m_n is the mass of the corresponding component, and m_t is the total mass of the missile for the dry or wet case. The calculated $c.g.$ are found in Table 3.

Table 3. Estimated Center of Gravity

Wet	165 cm
Dry	200 cm

The MOI for each of the components were calculated and added together using the equations given below.

Along the body's *X*-axis, the missile was assumed to be a cylinder and the fins and wings were assumed to be a point mass at a distance of 22 cm from the center line.

$$J_x = \sum_i \frac{1}{2} m_i r_i^2 + \sum_n m_n r_n^2 . \qquad \text{(eq. 37)}$$

Typically, with a missile, the body is symmetric about the *X*-axis, which means the MOI about the *Y* and *Z*-axis can be assumed to be same; $J_y = J_z$. For these axes, each body components' MOI was calculated as a cylinder. In addition, the parallel axis theorem was applied to account for the fact that the components $c.g.$ were not located at the c.g of the assembly. The shape of the fins and wings were then estimated as thin rectangles, and are subject to the parallel axis theorem as well.

$$J_y = J_z = \sum_i \frac{m_i}{12}(3r_i^2 + l_i^2) + m_i d_i^2 + \sum_n \frac{m_n}{12}(l_n^2 + h_n^2) + m_n d_n^2 . \qquad \text{(eq. 38)}$$

In both (eq. 37) and (eq. 38) *i* indexes the motor, warhead, and electronic and cone sections and *n* indexes the wings and fins.

Just like the *c.g.* a wet and dry MOI were calculated and are summarized in Figure 4

Table 4.   Estimated MOI for the AIM-120C

Axis	Wet ($kg\ m^2$)	Dry ($kg\ m^2$)
X	1.333	1.135
Y	266.4	224.7
Z	266.4	224.7

With all the necessary information collected, the next phase is to put the data into Missile DATCOM and record calculated aerodynamic coefficients.

B.   MISSILE DATCOM

Using the Missile DATCOM's user manual [7] as guidance, Missile parameters are inputted into the system by using a *for005.dat* file that can be edited with windows notepad. When the program is executed, the *for005.dat* information is read and any errors that may have been found are reported in the *for006.dat* file along with on the run. Missile DATCOM also produces an MS excel file label *for042*. This file contains the calculated coefficients for each of the different case in the for005.dat file.

To use Missile DATCOM, a series of MATLAB scripts were generated that would populate the *for005.dat* file with the current run parameters, run DATCOM, and extract the results from the *for042* MS excel. The process was repeated until a matrix of the aerodynamic coefficients was generated with the ranges seen in Table 5

Table 5.   Parameter Ranges for Calculating Aerodynamic Coefficients Using Missile DATCOM

Parameter	Range
Mach	0.1 to 4.0
Angle of attack (α)	-49° to 49°
Fin Deflection (δ)	-20° to 20°

Figure 8 shows the orientations that are used by Missile DATCOM when calculating the coefficients.
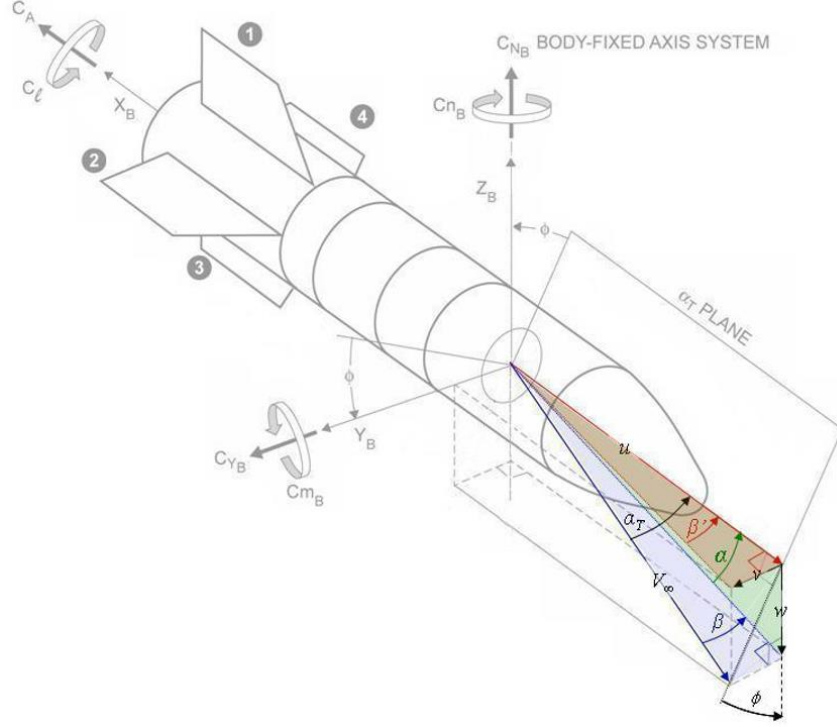
Figure 8. Missile DATCOM Orientations. Source: [6].

It can be seen that they are not the same as the orientation of our body frame. To correct this difference a rotation about the body y-axis was used applied to the aerodynamic coefficients calculated by Missile DATCOM,

$$\begin{bmatrix} CA \\ Cm \\ CN \end{bmatrix}^{b} = \begin{bmatrix} -1 & 0 & 0 \\ 0 & 1 & 0 \\ 0 & 0 & -1 \end{bmatrix} \begin{bmatrix} CA \\ Cm \\ CN \end{bmatrix}^{dm} . \tag{eq. 39}$$

C.   HIGH FIDELITY VS. LOW FIDELITY MODELS

One of the goals in this thesis is to show what level of model fidelity is required for developing a guidance with optimal control theory. The more "perfect" a model, the more complexity is required to developing an optimal guidance solution. In addition, it is difficult to account for all external disturbances that could possibly affect the real-world dynamics. A "good enough" model is one which allows a rapid optimal guidance

solution, and which allows RTOC to be applied. In this case there are two different models, a low-fidelity model used in developing the control, and a high-fidelity model to act as the real-world model. Our Missile DATCOM data will serve nicely as the high-fidelity model using the 3DOF equations, but the low-fidelity model needs to be determined.

As mentioned earlier, Zarchan provides a model for estimating Cn and Cm for Machs that are greater than supersonic speeds [5];

$$CN = 2\alpha + \frac{1.5 S_{plan}\alpha^2}{S_{ref}} + \frac{8 S_w \alpha^2}{B_e S_{ref}} + \frac{8 s_t (\alpha + \delta)}{B_e S_{ref}}$$

(eq. 40)

and

$$
\begin{aligned}
Cm = {} & 2\alpha(X_{cg} - X_{cpn}) + \frac{1.5 S_{plan}\alpha^2}{S_{ref}}(X_{cg} - X_{cpb}) \\
& + \frac{8 S_w \alpha}{B_e S_{ref}}(X_{cg} - X_{cpw}) + \frac{8 S_t (\alpha + \delta)}{B_e S_{ref}}(X_{cg} - X_{cpt})
\end{aligned}
$$

(eq. 41)

where X_{cg} is the location of the center of gravity. The remaining variables are defined by

$$
\begin{aligned}
S_{plan} &= Ld \\
S_{ref} &= \frac{\pi d^2}{4} \\
B_e &= \sqrt{Mach^2 - 1} \\
S_w &= 0.5 h_w (C_{tw} + C_{rw}) \\
S_t &= 0.5 h_t (C_{tt} + C_{rt})
\end{aligned}
$$

(eq. 42)

and their corresponding values are obtained by referencing Figure 9 and applying it to the missile.
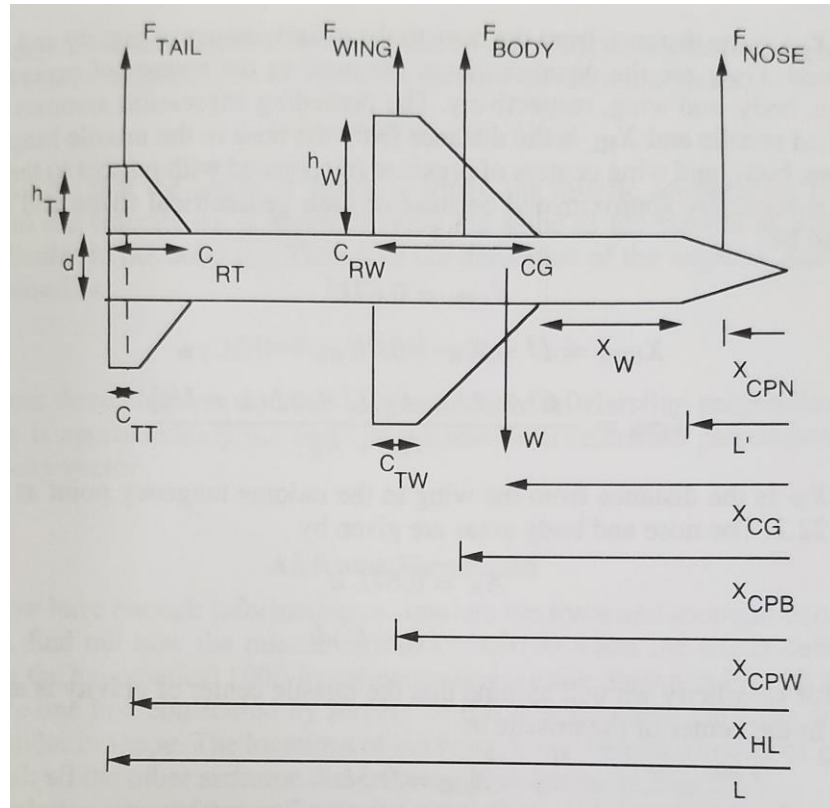
Figure 9. Forces on Tail-Controlled Missile. Source: [5].

Figure 10 shows that the values of coefficients derived from Zarchan are comparable to those obtain from Missile DATCOM when the angle of attack remains within $\pm 15°$.
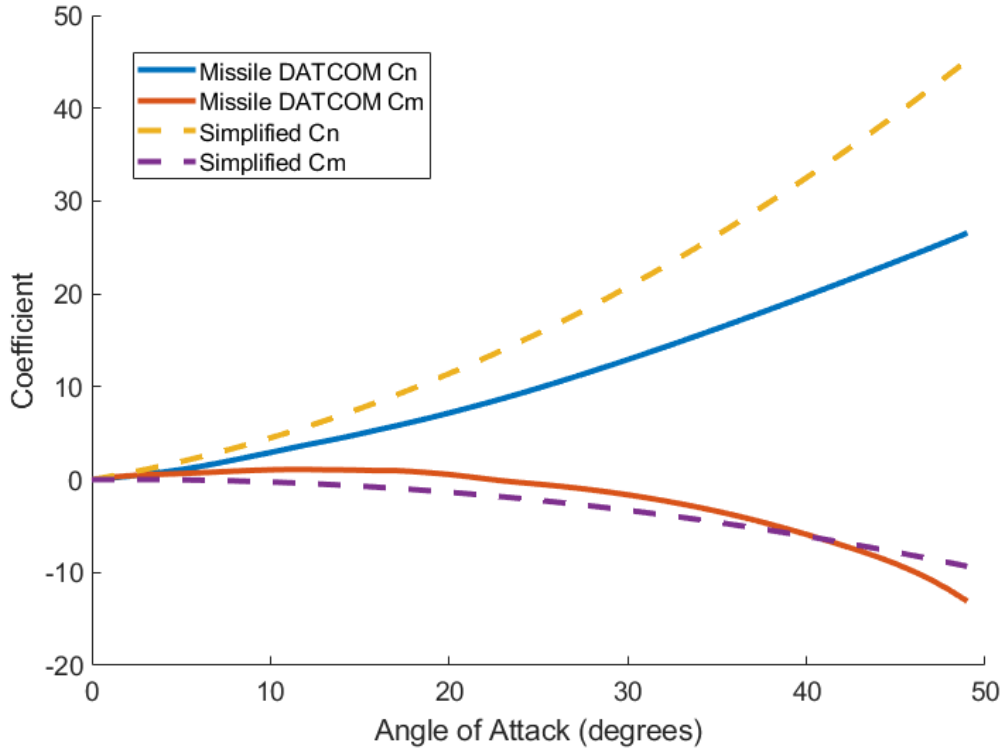
Figure 10.   Comparison of Missile DATCOM and Simplified
Coefficients

The axial coefficient (CA) was set to the average value obtained from Missile DATCOM, giving a value of $CA = -0.406$. Note that this will have implications in the missile performance: drag is independent of altitude, so there is no advantage in gaining altitude, and will have an impact on the optimal solution developed.

D.   FINS DEFLECTION

For a typical missile, the only form of control comes from fins that are known as control surfaces. These fins can be deflected at some angle (δ) to generate aerodynamic forces and moments on the body. This is true even during the boost phase because a missile typically does not have any control over the thrust direction in the body frame. The model in this thesis was simplified to have the control be the angular rate of the body's Y-axis (q). This simplification was done because the fin deflections operate at a rate much higher than the rest of the missile motion. The significant difference in rates

means that extra care is needed when numerically scaling the problem for DIDO to solve the boundary value problem. The concept of scaling is discussed later in section IV.B.2.

Having the control of the system being q assumes that the AIM-120 would be able to obtain those rates directly instead of having to manipulate the rear control surface to generate the necessary aerodynamic torque. However, one of the possible inputs to the Missile DATCOM tables are the fin deflections. If it is possible to calculate what kind of fin deflections that would generate the control, it would improve the model fidelity.

To solve for the fin deflection, we first reference back to 3-DOF equations found in equation (eq. 35), specifically the equation for $\dot{q}$,

$$\dot{q} = \frac{\overline{q} S_{ref} Cm}{I_{yy}},$$
(eq. 43)

then substituting equation (eq. 41) for Cm and then solve for δ,

$$\delta = \frac{\dot{q} I_{yy} B_e}{\overline{q} S_{ref} 12.107} - 0.2973 \alpha B_e + 1.147 \alpha^2 B_e + 0.8968 \alpha.$$
(eq. 44)

It is now possible to retroactively solve for what the fin deflections might have been, and then use that information to feed look-up tables supplying the coefficients for the high-fidelity model.

E. SUMMARY

This chapter covered the development of the physical characteristics of the missile, which were used to determined aerodynamic coefficients using Missile DATCOM. A simplified method for determining the coefficients was also introduced to act as the lower-fidelity model. The next chapter will address the concept of optimal control theory and how it is used to develop the optimal control.

THIS PAGE INTENTIONALLY LEFT BLANK

IV. OPTIMAL CONTROL THEORY

Pontryagin's principle on optimal control had its origins with his maximum principle [10]. Pontryagin's principle employed on an optimal control problem is to develop a boundary value problem, BVP, that, when solved, will provide the best, or optimal solution to the problem.

A. PROBLEM FORMULATION

The first step in solving the optimal control problem is to define the problem to be solved. As addressed earlier, the 3-DOF model is the basis of the guidance problem. This means that the states of the model will be $x = [X_e, Z_e, u, w, \theta]^T$. In addition, the control for the model will be defined as $\mu = [q]$. It is important to note that the standard notation for the control input is u. In this thesis μ is used to avoid confusion with the state variable u.

With the states defined, path constraints need to be developed and placed upon the trajectory. A path constraint is a function of the states and control of the system and is denoted by h. Upper and lower limits are placed on h, resulting in

$$h^{lowerbound} \leq h\big(x(.), \mu(.)\big) \leq h^{upperbound} \,. \tag{eq. 45}$$

The first path constraint will be placed upon the angle of attack (α), limiting it between $\pm 15°$. This path constraint was chosen because when α exceeds $\pm 15°$ Zarchan's approximation, (eq. 40) begins to diverge from the Missile DATCOM calculated aerodynamic coefficients.

Another constraint was placed upon the control to ensure that the control generated was one that the system would theoretically produce. In our model the control is the pitch rate. In reality, the controls for a missile in the midcourse phase are the deflections of the control surfaces, which produces a pitch acceleration,

$$\dot{q} = \frac{\overline{q}Cm(u,w,Z_e,\delta)}{I_y} \ . \qquad \text{(eq. 46)}$$

Solving for aerodynamic coefficient,

$$Cm = \frac{I_y\dot{q}}{\overline{q}} , \qquad \text{(eq. 47)}$$

it is possible to determine what value the aerodynamic coefficient needs to be to produce the desired pitch acceleration. The model was then allowed to be able to accelerate from the minimum pitch rate to the maximum pitch rate in 0.1 seconds, giving

$$\dot{q} = \frac{(q_{\max} - q_{\min})}{0.1} \ . \qquad \text{(eq. 48)}$$

If the pitch rate was bounded between ± 1.1 *radians/s* ($63^\circ / \text{s}$), at a height of 2000 meters, and velocity of 200 *m/s* the missile would then need to produce an aerodynamic coefficient of 13.96. Scanning through the calculated *Cm* from Missile DATCOM, at the velocity used and within the α bound, it is found that *Cm* of up to 23.18 is possible.

The path constraints are summarized as

$$\begin{aligned}
-15^\circ &\leq h_1(\alpha) \leq 15^\circ \\
-63^\circ / \text{s} &\leq h_2(q) \leq 63^\circ / \text{s}
\end{aligned} \qquad \text{(eq. 49)}$$

Next, the cost function and accompanying initial and final conditions need to be defined. The cost function is used to define the state(s) that affect the cost of the maneuver that is being performed by the system and is generally something that is minimized. It is defined as

$$J[x(.),\mu(.),t_f] = E(x(t_f),t_f) + \int_{t_o}^{t_f} F(x(t),\mu(t),t)dt , \qquad \text{(eq. 50)}$$

where $E(x(t_f),t_f)$ is the endpoint cost and $F(x(t),\mu(t),t)$ is the running cost.

The initial and final conditions can be either fixed or free, depending on the specific problem being considered. Throughout this thesis, three different cost functions

will be examined. For these cost functions, one set of initial conditions will satisfy the needs of all three cost functions. The initial conditions will be chosen to be $x(t_i) = [0, 2500m, 1528\frac{m}{s}, 0, \theta_i]$. A starting height of 2,500m was chosen as some height below the maximum cited ceiling for an F/A-18 Hornet, which is 15,240m [11]. The value $1528\frac{m}{s}$ is roughly Mach 4, for a height of 2000m. Mach 4 was chosen because it is the cited max speed of the AIM-120 [8]. The initial rotation of the body in the inertial frame, θ_i was left free.

The final conditions will be unique for each cost function. The first cost function will be to maximize the horizontal distance traveled, $J_1[x(.), \mu(.), t_f] = -X_e^f$. This cost function will be applied first the problem and using its solution as the frame work for the next two cost functions. For this cost function, a final condition of $x_1(t_f) = [X_e^f, 2000m, 200\frac{m}{s}, 0, \theta_f]$ was chosen. The final distance, X_e^f, is left open because it is the state that is being maximized. A final height of 2000 m was chosen just to be some height below the initial height. The final velocities were chosen by first setting 200 m/s as the minimum speed needed for a missile to be "capable" of hitting a target at the end of the mid-course phase. Second, all of the speed was desired to be in the direction the missile is pointed, $w_f = 0\frac{m}{s}$, $u_f = 200\frac{m}{s}$. The final rotation of the missile, θ_f, was then left free for the optimal control theory to determine.

The next cost function minimizes the final flight time, $J_2[x(.), \mu(.), t_f] = t_f$. The final conditions will be $x_2(t_f) = [\frac{2}{3}X_e^{max}, 2000m, 200\frac{m}{s}, 0, \theta_f]$, where X_e^{max} is the maximum distance obtained from the first cost function. This cost function is used to create a form of comparison for the results of the final cost function.

The last cost functions to be used will maximize the final kinetic energy by maximizing the final value of u_f, $J_3[x(.), \mu(.), t_f] = -u_f$. This cost function will be used to ultimately determine what the optimal trajectory would be for the missile. The

31

accompanying final conditions will then be $x_3(t_f) = [\frac{2}{3}X_e^{max}, 2000m, u_f, 0, \theta_f]$. X_e^{max} is

the same value as in $x_2(t_f)$.

The final problem will then be

$$p_i = \begin{cases} & x = [X_e, Z_e, u, w, \theta]^T \qquad \mu = [q] \\ \text{Minimize:} & J_i[x(.), \mu(.), t_f] \\ \\ \text{Subject to:} \quad f(x,u,t) = \begin{cases} \dot{X}_e = u\cos\theta + w\sin\theta \\ \dot{Z}_e = u\sin\theta - w\cos\theta \\ \dot{u} = \dfrac{F_u}{m} - qw - g\sin\theta \\ \dot{w} = \dfrac{F_w}{m} + qu + g\cos\theta \\ \dot{\theta} = -q \end{cases} \\ x(t_i) = [0, 2500, 1528, 0, \theta_i] \\ x_i(t_f) \\ -15^\circ \le h_1(\alpha) \le 15^\circ \\ -63^\circ/s \le h_2(q) \le 63^\circ/s \end{cases}$$

$$F_u = \bar{q}(u, w, Z_e)S_{ref}(-0.4060)$$
$$F_w = \bar{q}(u, w, Z_e)S_{ref}CN(u, w, Z_e) \qquad . \qquad \text{(eq. 51)}$$
$$CN = 2\alpha + \frac{1.5S_{plan}\alpha^2}{S_{ref}} + \frac{8S_w\alpha^2}{B_eS_{ref}} + \frac{8s_t\alpha}{B_eS_{ref}}$$
$$\alpha = -\tan^{-1}(\frac{w}{u})$$
$$\bar{q} = \frac{1}{2}\rho(Z_e)V^2$$
$$\rho = 1.225e^{-0.001184Z_e}$$

1. Derivation of the Necessary Conditions

Now that the problems have been formulated, it is possible to walk through the steps of the applying Pontryagin's principle of optimal control. We will first apply it to the problem set one.

a. Hamiltonian

The Hamiltonian is defined as [10]

$$H(\lambda, x, \mu, t) = F(x, \mu, t) + \lambda^T f(x, \mu, t). \qquad \text{(eq. 52)}$$

Consulting the cost function for the problem we find that there is no running cost, therefore, $F(x, u, t) = 0$. This leaves the Hamiltonian as a product of the co-vectors and dynamics,

$$H(\lambda, x, \mu, t) = \lambda^T f(x, \mu, t). \qquad \text{(eq. 53)}$$

The Hamiltonian has the units of $\dfrac{\text{cost-unit}}{\text{time-unit}}$ [10]. Note that state units cannot be added together to equal the cost-unit. This is where the co-vectors come in. The co-vectors, $\lambda = [\lambda_{X_e}, \lambda_{Z_e}, \lambda_u, \lambda_w, \lambda_\theta]^T$, have the units of $\dfrac{\text{cost-unit}}{\text{state-unit}}$ [10], where the state-unit corresponds to the co-vector's matching state. For example, λ_{X_e} has the units of $\dfrac{\text{cost-unit}}{\text{meters}}$, this is because its corresponding state, X_e, is measured with the units of meters. What this means is that as a result of the dot product between the co-vectors and dynamics, the Hamiltonian will have the units of $\dfrac{\text{cost-unit}}{\text{time-unit}}$ [10]. The Hamiltonian of the system is now

$$H(\lambda, x, u, t) = \lambda_{X_e}(u\cos\theta + w\sin\theta) + \lambda_{Z_e}(u\sin\theta - w\cos\theta) + \lambda_u(\frac{F_u}{m} - qw - g\sin\theta)$$
$$+ \lambda_w(\frac{F_w}{m} + qu + g\cos\theta) + \lambda_\theta(-q) \qquad \text{. (eq. 54)}$$

33

Next the Lagrangian of the Hamiltonian is established as

$$\bar{H}(\lambda, x, \mu, t) = H(\lambda, x, \mu, t) + l^T h. \qquad \text{(eq. 55)}$$

The Lagrangian of the Hamiltonian is important because it resolves issues when finding a local minimum created by the path constraints, h. This will be explained with more detail in the next section when the Hamiltonian is minimized. The symbol l, known as the Karush-Kuhn-Tucker multipliers (KKT), in this scenario is used in the same way that the co-vectors for the dynamics. In fact, they are co-vectors for the path constraints [10]. It is important to note that the standard notation for the KKT multipliers is μ and was changed to avoid confusion with the control, μ. The Lagrangian of the Hamiltonian can then be written as

$$\bar{H}(\lambda, x, \mu, t) = \lambda_{X_e}(u\cos\theta + w\sin\theta) + \lambda_{Z_e}(u\sin\theta - w\cos\theta)$$
$$+\lambda_u(\frac{F_u(u,w,Z_e,\delta)}{m} - qw - g\sin\theta) + \lambda_w(\frac{F_w(u,w,Z_e,\delta)}{m} + qu + g\cos\theta). \qquad \text{(eq. 56)}$$
$$+\lambda_\theta(-q) + l_1 h_1(\alpha) + l_2 h_2(q)$$

To minimize the Lagrangian of the Hamiltonian first the complementarity condition [10] must be met,

$$l_i \begin{cases} \leq 0 & if & h_i = h^{\min} \\ = 0 & if & h^{\min} < h_i < h^{\max} \\ \geq 0 & if & h_i = h^{\max} \end{cases}. \qquad \text{(eq. 57)}$$

This means that if the scenario never hits the path constraints the KKT multipliers will remain zero, and the Lagrangian of the Hamiltonian will be equivalent to the Hamiltonian. Note, the complementarity condition does not prevent the system from reaching the path constraints or even "ride" them for a time. Applied to the problem, the complementarity conditions are

$$l_1 \begin{cases} \leq 0 & if & h_1(\alpha) = -15° \\ = 0 & if & -15° < h_1(\alpha) < 15° \\ \geq 0 & if & h_1(\alpha) = 15° \end{cases}$$
$$l_2 \begin{cases} \leq 0 & if & h_2(q) = -63° / s \\ = 0 & if & -63° / s < h_2(q) < 63° / s \\ \geq 0 & if & h_2(q) = 63° / s \end{cases}$$

(eq. 58)

b.   *Minimizing the Hamiltonian*

The intent of this process is to find the lowest cost, *J*, of the problem formulated. This means finding the control that produces the smallest change in cost over time, for all time, will result in the lowest overall cost. Remembering that the Hamiltonian is $\frac{\text{cost-unit}}{\text{time-unit}}$, then finding the minimum of the Hamiltonian with respect to the control will result in the lowest overall cost for the maneuver. Figure 11 helps demonstrate this point.
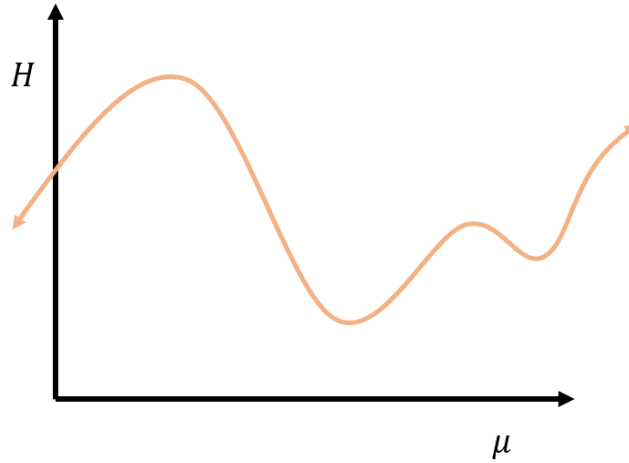

Figure 11.   Hypothetical Hamiltonian vs. Control. Adapted from [10]

The local candidate minimums can then be identified when

$$\frac{\partial H}{\partial \mu} = 0.$$

(eq. 59)

35

Equation (eq. 59) is known as minimizing the Hamiltonian. This, however, is only part of the story, because in Figure 11 the control, μ, does not have any bounds placed upon it equation (eq. 59) is enough to capture all possible solutions. But if the control does have bounds placed upon it, such as a path constraint, then equation (eq. 59) is not sufficient [10]. This is seen in Figure 12.
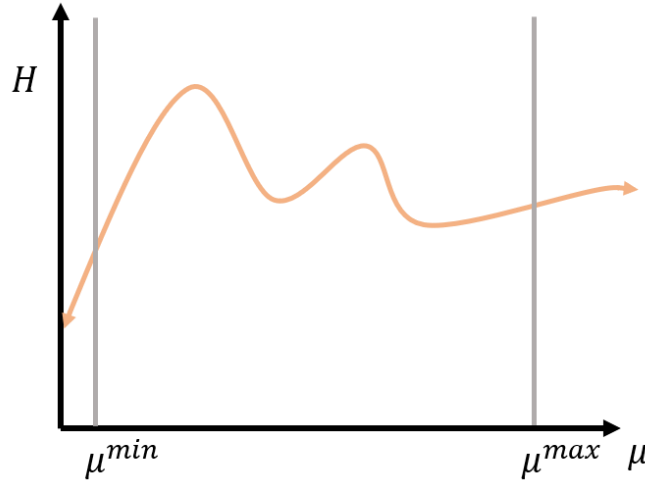

Figure 12.   Hypothetical Hamiltonian vs. Control w/ Bounds.
Adapted from [10].

If only the points where the slope is zero are taken as possible solutions, then the actual solution, located at the control's minimum, will be missed. This is where the Lagrangian of the Hamiltonian comes in. Because the Lagrangian considers path constraints, it can be used to solve for the solution. This also brings up another condition for minimizing the Lagrangian, the stationarity condition [10], which is defined as

$$\frac{\partial \bar{H}}{\partial \mu} = 0. \tag{eq. 60}$$

Applying this to our problem,

$$\frac{\partial \bar{H}}{\partial \mu} = \frac{\partial H}{\partial q} + \frac{\partial (l^T h)}{\partial q} = 0 = -\lambda_u w + \lambda_w u - \lambda_\theta + l_2. \tag{eq. 61}$$

36

Referring to equation (eq. 58) it can be seen that as long as the control is not located at the bounds, l_2 will be zero and minimizing the Lagrangian of the Hamiltonian becomes equivalent to minimizing the Hamiltonian,

$$\frac{\partial \bar{H}}{\partial \mu} = \frac{\partial H}{\partial q} = 0 = -\lambda_u w + \lambda_w u - \lambda_\theta . \qquad \text{(eq. 62)}$$

c.   Adjoints

With the Lagrangian of the Hamiltonian minimized, the next step is to find the adjoints. In solving the optimal control problem, the values of the co-vectors ultimately need to be determined. To do this we must first determine what the dynamics of the co-vectors are. This is where the adjoints come in. To solve for the adjoints [10]

$$\frac{\partial H}{\partial x} = -\dot{\lambda}_x . \qquad \text{(eq. 63)}$$

Applying this to each state of the problem yields

$$
\begin{aligned}
\dot{\lambda}_{X_e} &= 0 \\[4pt]
\dot{\lambda}_{Z_e} &= -(\lambda_u \frac{\partial F_u}{\partial Z_e(m)} + \lambda_w \frac{\partial F_w}{\partial Z_e(m)}) \\[4pt]
\dot{\lambda}_u &= -(\lambda_{X_e} \cos\theta + \lambda_{Z_e} \sin\theta + \lambda_u \frac{\partial F_u}{\partial u(m)} + \lambda_w (\frac{\partial F_w}{\partial u(m)} + q) + l_1 \frac{2w}{u^2} \sec^2 \frac{w}{u}) \\[4pt]
\dot{\lambda}_w &= -(\lambda_{X_e} \sin\theta - \lambda_{Z_e} \cos\theta + \lambda_u (\frac{\partial F_u}{\partial w(m)} - q) + \lambda_w (\frac{\partial F_w}{\partial w(m)}) + l_1 \frac{1}{u} \sec^2 \frac{w}{u}) \\[4pt]
\dot{\lambda}_\theta &= -(\lambda_{X_e} (-u \sin\theta + w \cos\theta) + \lambda_{Z_e} (u \cos\theta + w \sin\theta) - \lambda_u g \cos\theta - \lambda_w g \sin\theta
\end{aligned}
\qquad \text{. (eq. 64)}
$$

One immediate take away that we can see is that λ_{X_e} is a constant, which will be an important means of validation and verification later when the optimal control problem is solved. Next, we then need to calculate the partials derivative of the forces with respect to each state,

37

$$\frac{\partial F_u}{\partial u} = \rho(Z_e)uS_{ref}CN$$

$$\frac{\partial F_u}{\partial w} = \rho(Z_e)wS_{ref}CN$$

$$\frac{\partial F_u}{\partial Z_e} = -0.0007252e^{-0.001184Z_e}V^2 S_{ref}CA$$

$$\frac{\partial F_w}{\partial u} = \rho(Z_e)uS_{ref}CN$$ (eq. 65)

$$\frac{\partial F_w}{\partial w} = \rho(Z_e)wS_{ref}CN$$

$$\frac{\partial F_w}{\partial Z_e} = -0.0007252e^{-0.001184Z_e}V^2 S_{ref}CN$$

Combining equations (eq. 64) and (eq. 65) the adjoints for the problem are obtained,

$$\dot{\lambda}_{X_e} = 0$$

$$\dot{\lambda}_{Z_e} = -\left(-\lambda_u 0.0007252e^{-0.001184Z_e}\frac{V^2}{m}S_{ref}CA - \lambda_w 0.0007252e^{-0.001184Z_e}\frac{V^2}{m}S_{ref}CN\right)$$

$$\dot{\lambda}_u = -\left(\lambda_{X_e}\cos\theta + \lambda_{Z_e}\sin\theta + \lambda_u\frac{\rho(Z_e)uS_{ref}CA}{m}\right.$$
$$\left. +\lambda_w\left(\frac{\rho(Z_e)uS_{ref}Cn}{m}+q\right)+l_1\frac{2w}{u^2}\sec^2\frac{w}{u}\right)$$. (eq. 66)

$$\dot{\lambda}_w = -\left(\lambda_{X_e}\sin\theta - \lambda_{Z_e}\cos\theta - \lambda_u\left(\frac{\rho(Z_e)wS_{ref}CA}{m}+q\right)\right.$$
$$\left. +\lambda_w\left(\frac{\rho(Z_e)wCN}{m}\right)+l_1\frac{1}{u}\sec^2\frac{w}{u}\right)$$

$$\dot{\lambda}_\theta = -\left(\lambda_{X_e}(-u\sin\theta + w\cos\theta) + \lambda_{Z_e}(u\cos\theta + w\sin\theta) - \lambda_u g\cos\theta - \lambda_w g\sin\theta\right)$$

d. Transversality

Now that the dynamics of the co-states have been determined, that last step before constructing the boundary value problem is to solve for the transversality conditions. The transversality equation is found by using the endpoint Lagrangian [10],

$$\bar{E}(x(t_f),t_f) = E(x(t_f),t_f) + v^T e(x_f,t_f).$$ (eq. 67)

The equation $E(x(t_f), t_f)$ is found by referring to equation (eq. 50) and the cost function chosen for the problem. $e(x(t_f), t_f)$ is obtained by the endpoint conditions established in the problem formulation,

$$e(x(t_f), t_f) = \begin{bmatrix} Z_e(t_f) - 2000 \\ u(t_f) - 200 \\ w(t_f) - 0 \end{bmatrix}. \tag{eq. 68}$$

Where the vector ν is another set of co-vectors, $[\nu_1, \nu_2, \nu_3]$. This results in

$$\bar{E}(x(t_f), t_f) = -X_{e_f} + \nu_1(Z_{e_f} - 2000) + \nu_2(u_f - 200) + \nu_3(w_f - 0). \tag{eq. 69}$$

With the endpoint Lagrangian, it is then might be possible to determine some of the λ co-vector final time values [10],

$$\frac{\partial \bar{E}}{\partial x_f} = \lambda(t_f). \tag{eq. 70}$$

The endpoint Lagrangian may not provide the final time value for all the λ co-vectors, nor is it guaranteed to provide any at all. When applied to the current problem

$$\begin{aligned} \lambda_{X_e}(t_f) &= -1 \\ \lambda_{Z_e}(t_f) &= \nu_1 \\ \lambda_u(t_f) &= \nu_2 \\ \lambda_w(t_f) &= \nu_3 \end{aligned} \tag{eq. 71}$$

In this problem, the only useful information that comes from solving the transversality is that the $\lambda_{X_e}(t_f) = -1$. This is because the value of X_{e_f} is not specified and is the cost of the problem. Coupled with the knowledge that $\dot{\lambda}_{X_e} = 0$ we also know that $\lambda_{X_e}(t_0) = -1$. In this problem, the endpoint Lagrangian turned out to be useful.

2. Constructing BVP

Now that we have completed all the supporting steps, the final phase is the put the BVP together

$$
\begin{bmatrix}
\dot{X}_e = u\cos\theta + w\sin\theta \\
\dot{Z}_e = u\sin\theta - w\cos\theta \\
\dot{u} = \dfrac{F_u}{m} - qw - g\sin\theta \\
\dot{w} = \dfrac{F_w}{m} + qu + g\cos\theta \\
\dot{\theta} = -q
\end{bmatrix}
$$

$$x(t_o) = [0, 2000, 1528, 0, \theta_o]$$
$$x_1(t_f) = [X_e^f, 2000, 200, 0, \theta_f]$$

$$
\begin{bmatrix}
\dot{\lambda}_{X_e} = 0 \\[2mm]
\dot{\lambda}_{Z_e} = -\left(-\lambda_u 0.0007252 e^{-0.001184 Z_e} \dfrac{V^2}{m} S_{ref} CA - \lambda_w 0.0007252 e^{-0.001184 Z_e} \dfrac{V^2}{m} S_{ref} CN\right) \\[2mm]
\dot{\lambda}_u = -\Bigg(\lambda_{X_e}\cos\theta + \lambda_{Z_e}\sin\theta + \lambda_u \dfrac{\rho(Z_e)uS_{ref}CA}{m} \\[2mm]
\quad + \lambda_w\left(\dfrac{\rho(Z_e)uS_{ref}Cn}{m} + q\right) + l_1 \dfrac{2w}{u^2}\sec^2\dfrac{w}{u}\Bigg) \\[2mm]
\dot{\lambda}_w = -\Bigg(\lambda_{X_e}\sin\theta - \lambda_{Z_e}\cos\theta - \lambda_u\left(\dfrac{\rho(Z_e)wS_{ref}CA}{m} + q\right) \\[2mm]
\quad + \lambda_w\left(\dfrac{\rho(Z_e)wCN}{m}\right) + l_1 \dfrac{1}{u}\sec^2\dfrac{w}{u}\Bigg) \\[2mm]
\dot{\lambda}_\theta = -\big(\lambda_{X_e}(-u\sin\theta + w\cos\theta) + \lambda_{Z_e}(u\cos\theta + w\sin\theta) - \lambda_u g\cos\theta - \lambda_w g\sin\theta
\end{bmatrix}
$$
. (eq. 72)

$$\lambda(t_o) = [-1, \lambda_{Z_e}^o, \lambda_u^o, \lambda_w^o, \lambda_\theta^o]$$
$$\lambda(t_f) = [-1, \lambda_{Z_e}^f, \lambda_u^f, \lambda_w^f, \lambda_\theta^f]$$
$$[t_o, t_f] = [0, t^f]$$

To solve a set of BVP of N equations, N point conditions are also needed [10]. In addition to the N point conditions initial and final propagating times are also needed, meaning a total of $N+2$ point conditions are required to the solve the BVP developed in

40

the optimal control problem. Looking at equation (eq. 72) we can see that we have ten equations, with ten known point conditions, meaning that we are missing 2 point conditions. If referring to equation (eq. 61) it is possible to obtain the two missing point conditions. When solving equation (eq. 61) for λ_w

$$\lambda_w = \frac{\lambda_u w - \lambda_\theta + l_2}{u}. \qquad \text{(eq. 73)}$$

And then solve (eq. 73) at time t_o and t_f,

$$\lambda_w(t_o) = \frac{-\lambda_\theta(t_o) - l_2(t_o)}{1528}$$
$$\lambda_w(t_f) = \frac{-\lambda_\theta(t_f) - l_2(t_f)}{200}. \qquad \text{(eq. 74)}$$

This then provides the last point conditions.

B.   SOLVING THE BOUNDARY VALUE PROBLEM

Now that the BVP has been developed, it needs to be solved. The methods to solve a BVP vary quite significantly and are a field of study all their own. Some methods include using a fixed-point iteration, where a possible solution is guessed at, and the refined with each iteration. The problem with this method is that it requires a good initial guess at what the solution would be, otherwise the method may never converge on the solution. Many other types of methods and programs are available to help in solving these types of problems. For this research, the program DIDO [10] was employed.

1.   DIDO

DIDO is unique in that it is designed to specifically solve BVPs developed using Pontryagin's principle for optimal control theory. As standard outputs, DIDO produces the values of the Hamiltonian, the co-vectors, and even the KKT multipliers for the path constraints, in addition to the values of the system states. DIDO can solve these problem, when properly scaled, in minutes or even less.

2. Scaling and Balancing

The key to using DIDO, other than ensuring the dynamics are properly coded, is to scale and balance the problem. Scaling can be applied allowing each of the states to have a custom unit applied to it that is more accommodating for the problem at hand. An example of properly scaling a problem would be if in X-axis you are traveling in km/s, while Y-axis you are traveling in m/s. if both axes are measured in km then change in the Y-axis may go unnoticed, or even uncalculated due to algorithmic tolerances. This can be a problem especially if that change in meters along the Y-axis is important to the problem at whole. This "problem" can be resolved by allowing the Y-axis to be measure in meters, while allowing the X-axis to be measure in kilometers.

Scaling also affects DIDO because of the interactions of the co-vectors and the states. Initially, the range of values that the co-vectors could take are unknown, and to an extent so are the states. This could mean that a co-state could take on a value several times larger, or smaller, than that of the corresponding states. A significant difference means that small changes in either the state or co-state may not register and can be lost in DIDO. This can cause DIDO to take significantly longer to solve the problem, if it can even solve it all.

To apply scaling to our problem first the relationship between the states and their scaling is established,

$$\bar{X}_e = \frac{X_e}{XU} \quad \bar{Z}_e = \frac{Z_e}{ZU}$$

$$\bar{u} = \frac{u}{UU} \quad \bar{w} = \frac{w}{WU}$$

$$\bar{\theta} = \frac{\theta}{THU} \quad \bar{t} = \frac{t}{TU} \qquad \text{(eq. 75)}$$

$$\bar{q} = \frac{q}{QU}$$

Where $[\bar{X}_e, \bar{Z}_e, \bar{u}, \bar{w}, \bar{\theta}, \bar{t}]$ represent the scaled states and $[XU, ZU, UU, WU, THU, TU]$ represent to scaling used. Next the dynamics need to be scaled. Using

$$\dot{X}_e = \frac{dX_e}{dt} = \frac{\dfrac{d\bar{X}_e}{XU}}{\dfrac{d\bar{t}}{TU}} = \frac{d\bar{X}_e}{d\bar{t}}\left(\frac{TU}{XU}\right) = \dot{\bar{X}}_e\left(\frac{TU}{XU}\right), \qquad \text{(eq. 76)}$$

Provides the scaled dynamics. Applying the scaled states and dynamics to the problem,

$$x = [\bar{X}_e, \bar{Z}_e, \bar{u}, \bar{w}, \bar{\theta}]^T \qquad \mu = [\bar{q}]$$

$$p_1 = \begin{cases}
\text{Minimize:} \qquad \bar{J}_1[\bar{x}(.), \bar{u}(.), \bar{t}_f] = -\bar{X}_e^f \\[2mm]
\text{Subject to:} \quad f(x,u,t) = \begin{cases}
\dot{\bar{X}}_e = (\bar{u}UU\cos(\bar{\theta}THU) + \bar{w}WU\sin(\bar{\theta}THU))\dfrac{TU}{XU} \\[2mm]
\dot{\bar{Z}}_e = (\bar{u}UU\sin(\bar{\theta}THU) - \bar{w}WU\cos(\bar{\theta}THU))\dfrac{TU}{ZU} \\[2mm]
\dot{\bar{u}} = (\dfrac{\bar{F}_u}{m} - \bar{q}QU\bar{w}WU - g\sin(\bar{\theta}THU))\dfrac{TU}{UU} \\[2mm]
\dot{\bar{w}} = (\dfrac{\bar{F}_w}{m} + \bar{q}QU\bar{u}UU + g\cos(\bar{\theta}THU))\dfrac{TU}{WU} \\[2mm]
\dot{\bar{\theta}} = (-\bar{q}QU)\dfrac{TU}{THU}
\end{cases} \\[20mm]
[\bar{t}_o, \bar{t}_f] = [\dfrac{0}{TU}, \dfrac{t^f}{TU}] \\[2mm]
\bar{x}(t_o) = [\dfrac{0}{XU}, \dfrac{2000}{ZU}, \dfrac{1528}{UU}, \dfrac{0}{WU}, \bar{\theta}_o] \\[2mm]
\bar{x}_1(t_f) = [\bar{X}_e^f, \dfrac{2000}{ZU}, \dfrac{200}{UU}, \dfrac{0}{WU}, \bar{\theta}_f] \\[2mm]
-15^\circ \le h_1(\bar{\alpha}) \le 15^\circ \\[2mm]
\dfrac{-63^\circ/\text{s}}{QU} \le h_2(\bar{q}) \le \dfrac{63^\circ/\text{s}}{QU}
\end{cases}$$

$$\bar{F}_u = \bar{\bar{q}}(\bar{u}, \bar{w}, \bar{Z}_e)S_{ref}(-0.4060)$$
$$\bar{F}_w = \bar{\bar{q}}(\bar{u}, \bar{w}, \bar{Z}_e)S_{ref}Cn(\bar{u}, \bar{w}, \bar{Z}_e)$$
$$CN = 2\alpha + \frac{1.5S_{plan}\alpha^2}{S_{ref}} + \frac{8S_w\alpha^2}{B_e S_{ref}} + \frac{8s_t\alpha}{B_e S_{ref}}$$
$$\bar{\alpha} = -\tan^{-1}(\frac{\bar{w}WU}{\bar{u}UU})$$
$$\bar{\bar{q}} = \frac{1}{2}\rho(\bar{Z}_e)|\bar{V}|^2$$
$$\bar{V} = \sqrt{(\bar{u}UU)^2 + (\bar{w}WU)^2} \qquad\qquad \text{(eq. 77)}$$
$$\bar{\rho} = 1.225e^{-0.001184\bar{Z}_e ZU}$$

At this point the complete process of determining the Hamiltonian, the adjoint equations, and transversality will be conducted again. While it is not necessary to show the process again, there is one aspect of note, and that is with the co-vectors, λ. Recall

back in section IV.A.1.a that the co-vectors have the units of $\dfrac{\text{cost-unit}}{\text{state-unit}}$. When constructing the scaled Hamiltonian, the co-vectors then need to have the units of $\dfrac{\text{cost-unit}}{\text{scaled-state-unit}}$, $\bar{\lambda}$. If proceeding similarly to the way the states were scaled,

$$n_c = NV_c\dot{\lambda}_{los} \qquad\qquad \text{(eq. 78)}$$

$$\text{scaled-state-unit} = \frac{\text{state-unit}}{\text{scale}} \qquad\qquad \text{(eq. 79)}$$

This resulting in

$$\bar{\lambda} = \text{scale} * \lambda . \qquad\qquad \text{(eq. 80)}$$

What this means that if the scaled state is smaller than the state then the scaled co-state will be larger than the co-state, and vice-versa. This is the balance. The scales used for the states need to be picked in such a way that the states and co-states are close enough to each other that difference can be noticed.

C.   VALIDATION AND VERIFICATION

After obtaining the optimal solution, the results need to be verified. First the control is propagated through the same dynamical model that was used to obtain the optimal control solution. The propagation test ensures that a converged DIDO solution employed a sufficient number of nodes. For the maximum range problem, only a small number of nodes was needed to obtain a useable solution and makes demonstrating the impact of having too few nodes difficult. Figure 13 and Figure 14 show the differences between a 20 nodes solution and a 120 node solution. Table 6 shows the difference in the final position of the propagated solutions as compared to the desired final position. For other problems these differences could be significant enough that the higher node solution is required.
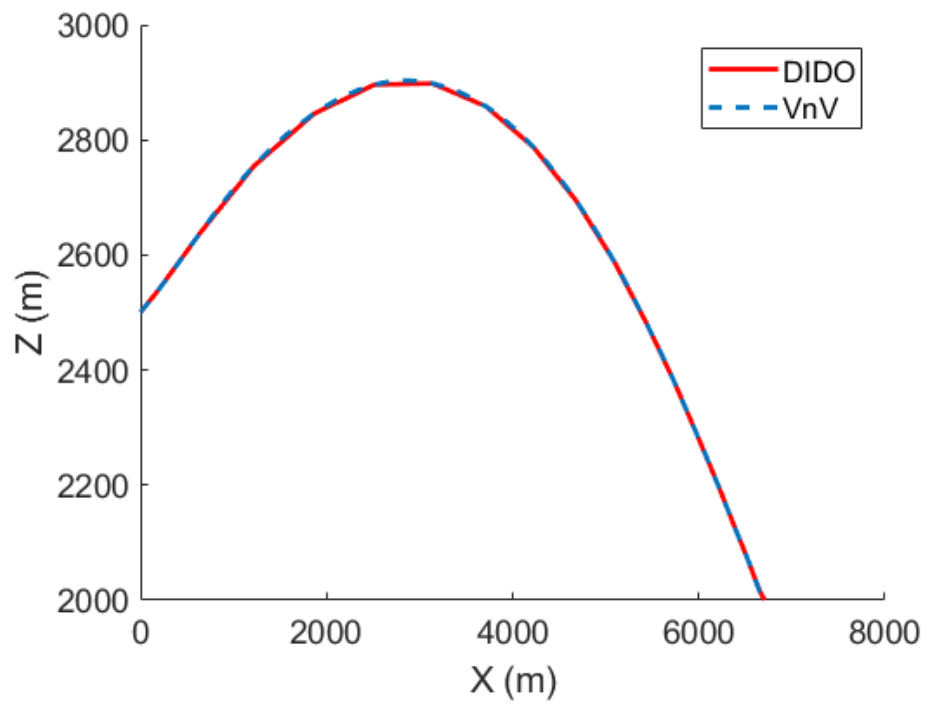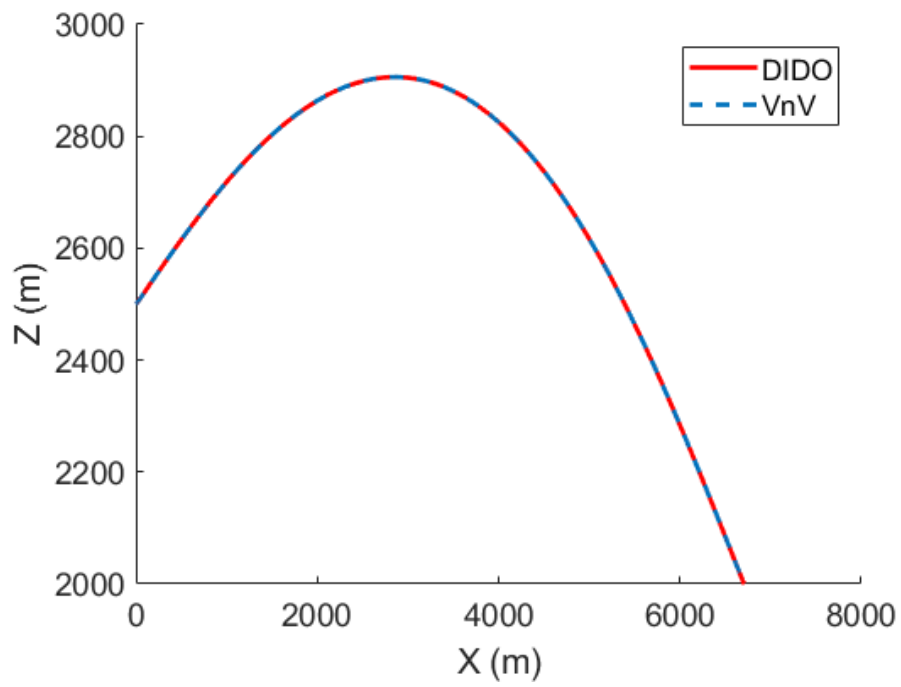
Figure 13.   Max Range Propagation with 20 Nodes

Figure 14.   Max Range Propagation with 120 Nodes

Table 6.   Summary of Impact of Nodes on Propagation

Number of Nodes	Miss Distance (m)
20	0.45
120	0.02

Another validation that was mentioned earlier was the value and dynamics of the co-state λ_{Xe}, in that it should be at a constant value of -1. Figure 15 shows the values of values of the co-states, as determined by DIDO, and we can see that $\lambda_{X_e}(t_f) = -1$ is obtained.
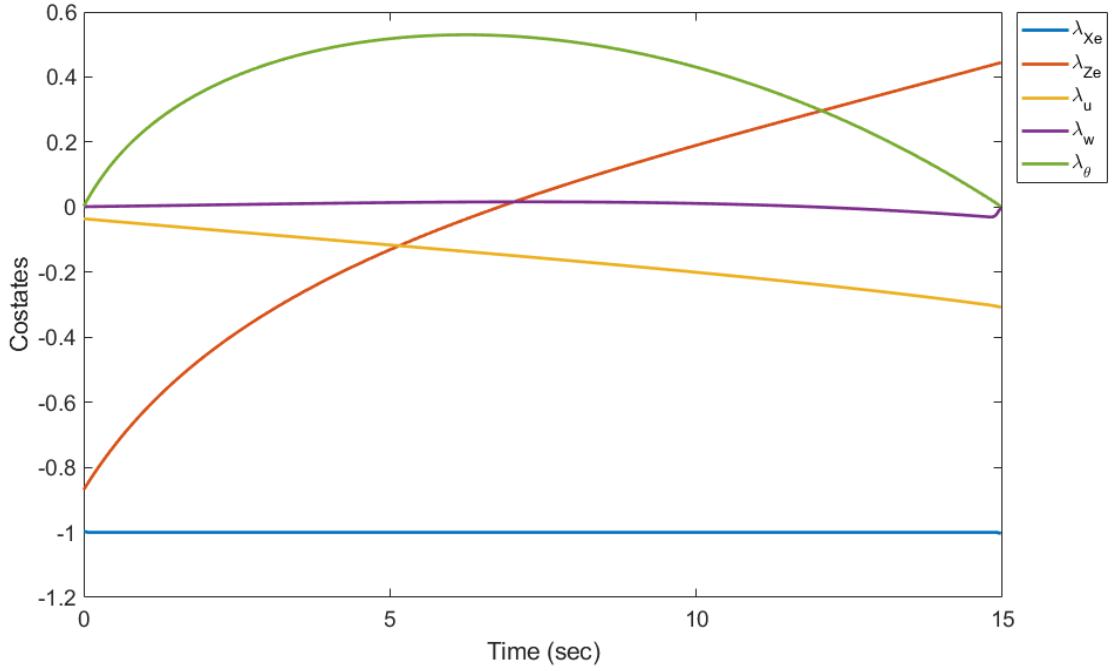
Figure 15.   Costates for the Maximum Range Solution

D.   SUMMARY

In this chapter, the optimal control process was addressed; setting up the problem, finding the Lagrangian of the Hamiltonian, minimizing the problem, solving for the adjoints, and solving for the transversality requirements. The resulting boundary value

problem was then solved using the solver known as DIDO, which introduced the concept of scaling and balancing. Finally, the results solution from DIDO was validated and verified by propagating the solution with the same dynamics used to obtain the optimal solution. In addition, the resulting costates were also cross checked with expected performance from the adjoints and transversality. The next chapter will then introduce the Proportional Navigation control laws and how they were implemented in the simulation.

THIS PAGE INTENTIONALLY LEFT BLANK

V.   PROPORTIONAL NAVIGATION

Since the inception of the tactical missile guidance after World War II, proportional navigation has seen a significant research effort to improve its performance, mainly in defining the gains used. Much of this work has been summarized in Balakrishnan, *et al.* [2]. To provide a baseline for comparison, the basic concepts of proportional navigation as summarized by Zarchan [5] will be implemented as an example of a standard control method.

A.   CONTROL LAW DERIVATION

Figure 16 shows the basic geometry that will be used in the proportional navigation law.
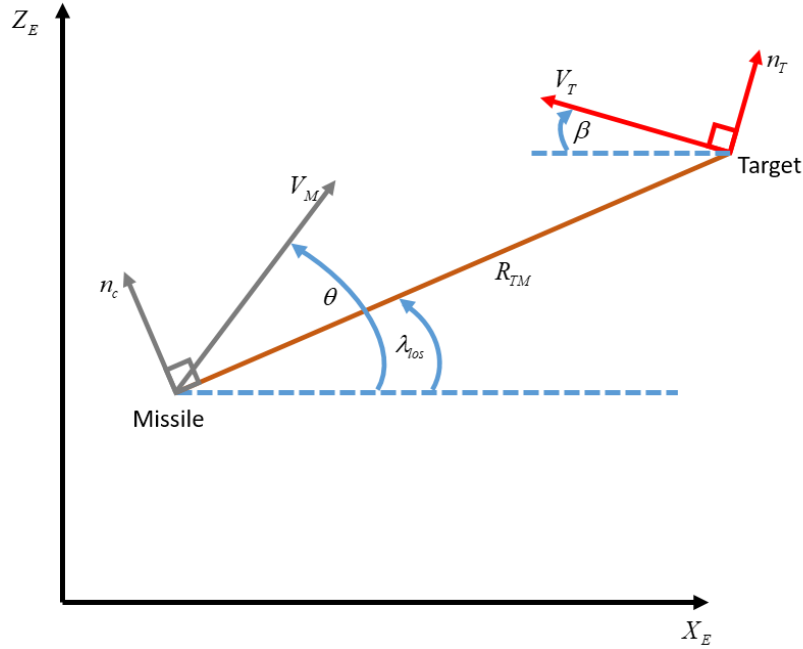
Figure 16.   Missile-Target Engagement Geometry. Adapted from [5].

In Figure 16 λ_{los} is the line of sight between the missile and the target, R_{TM} is then range between the missile and target. V_M is the velocity of the missile, n_c is the

49

acceleration of the missile perpendicular to the line of sight, V_T is the velocity of the target, and n_T is the acceleration of the target perpendicular to its velocity [5]. The guidance law is then stated as

$$n_c = NV_c \dot{\lambda}_{los} \qquad \text{(eq. 81)}$$

Where N is the effective navigation ratio, or the gain and V_c is the missile-target closing velocity, $V_c = -\dot{R}_{TM}$ [5].

If the coordinates of the missile are defined as

$$\begin{bmatrix} X_e \\ Z_e \end{bmatrix} = \begin{bmatrix} R_{MX_e} \\ R_{MZ_e} \end{bmatrix}, \qquad \text{(eq. 82)}$$

and the target as

$$\begin{bmatrix} X_e \\ Z_e \end{bmatrix} = \begin{bmatrix} R_{TX_e} \\ R_{TZ_e} \end{bmatrix}, \qquad \text{(eq. 83)}$$

then missile-target range can be defined as [5]

$$\begin{aligned} R_{TMX_e} &= R_{MX_e} - R_{TX_e} \\ R_{TMZ_e} &= R_{MZ_e} - R_{TZ_e} \\ R_{TM} &= \sqrt{R_{TMX_e}^2 + R_{TMZ_e}^2} \end{aligned} \qquad \text{(eq. 84)}$$

Using Figure 16 as a reference, the velocities of the missile are then defined as

$$\begin{aligned} V_{MX_e} &= V_M \cos\theta \\ V_{MZ_e} &= V_M \sin\theta \end{aligned} \qquad \text{(eq. 85)}$$

Similarly, the target velocities are

50

$$V_{TX_e} = V_T \cos \theta$$
$$V_{TZ_e} = V_T \sin \theta$$

$$(\text{eq. 86})$$

The relative velocities may then be computed,

$$V_{TMX_e} = V_{MX_e} - V_{TX_e}$$
$$V_{TMZ_e} = V_{MZ_e} - V_{TZ_e}$$

$$(\text{eq. 87})$$

Finally, the closing velocity is defined as [5]

$$V_c = -\frac{R_{TMX_e} V_{TMX_e} + R_{TMZ_e} V_{TMZ_e}}{R_{TM}}$$

$$(\text{eq. 88})$$

It is possible to define the line of sight rate as [5]

$$\dot{\lambda}_{los} = \frac{R_{TMX_e} V_{TMZ_e} - R_{TMZ_e} V_{TMX_e}}{R_{TM}^2}$$

$$(\text{eq. 89})$$

However, this is only good for small angles approximation. In this simulation, Simulink's capabilities were leveraged to calculate the line of sight angle rate for the control.

Finally, the value of gain N is chosen to be a constant, usually between 3 and 5 [5]. The output of the control law is then an acceleration perpendicular to the line of sight. Defining the line of sight as [5]

$$\lambda_{los} = \tan^{-1} \frac{R_{TMZ_E}}{R_{TMX_E}},$$

$$(\text{eq. 90})$$

it is possible to convert the acceleration to the inertial frame as

$$\dot{R}_{MX_e} = -n_c \sin \lambda$$
$$\dot{R}_{MZ_e} = n_c \cos \lambda$$

$$(\text{eq. 91})$$

This control is converted into a control useable by the model the dynamics defined in Chapter II, Section D, specifically where the acceleration in the inertial frame is defined as

$$\dot{R}_{MX_e} = \dot{X}_e = u\cos\theta + w\sin\theta$$
$$\dot{R}_{MZ_e} = \dot{Z}_e = u\sin\theta - w\cos\theta$$
.
(eq. 92)

Solving for θ,

$$\theta_d = \sin^{-1}\left(\frac{\dot{R}_{MZ_e} + \dfrac{w\dot{R}_{MX_e}}{u}}{\left(u - \dfrac{w^2}{u}\right)}\right).$$
(eq. 93)

Equation (eq. 93) provides a desired pitch, θ_d, which allows for the sensed pitch to be feed back to the input,

$$q = k(\theta_d - \theta),$$
(eq. 94)

where k is a proportional gain.

With a useable control in for the model from the proportional navigation method, a test was conducted using the initial conditions obtained from maximum range problem and the derived range of 6478 m and $N = 3$ and $k = 1$. For this test, and other future test, the target was assumed to be stationary. This first attempt at proportional navigation did not end in success, Figure 17 shows this result.
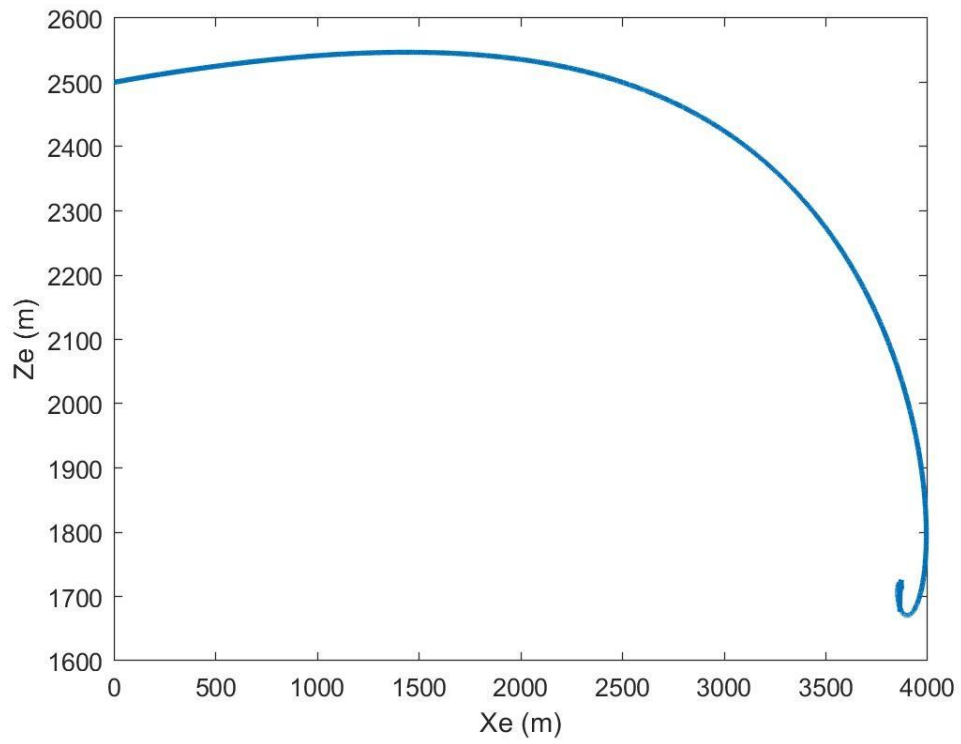
Figure 17.   Simulation of Proportional Navigation with $N = 3$ and $k = 1$

After spending some time adjusting the value of the proportional gain, k, it was found that $k = 0.2$ produced a workable solution, as seen in Figure 18.
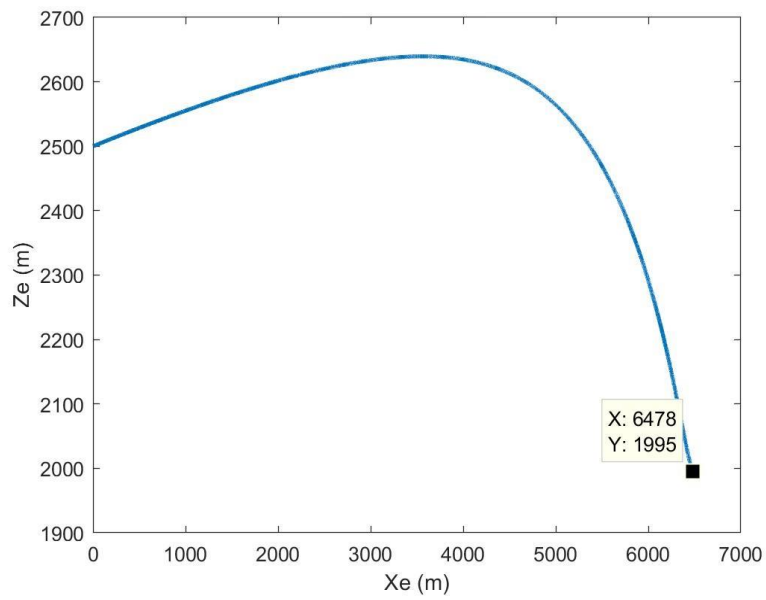
Figure 18.　　Simulation of Proportional Navigation with $N = 3$ and k $= 0.2$

Figure 19 and Figure 20 show the accompanying line of sight and control for the simulation.
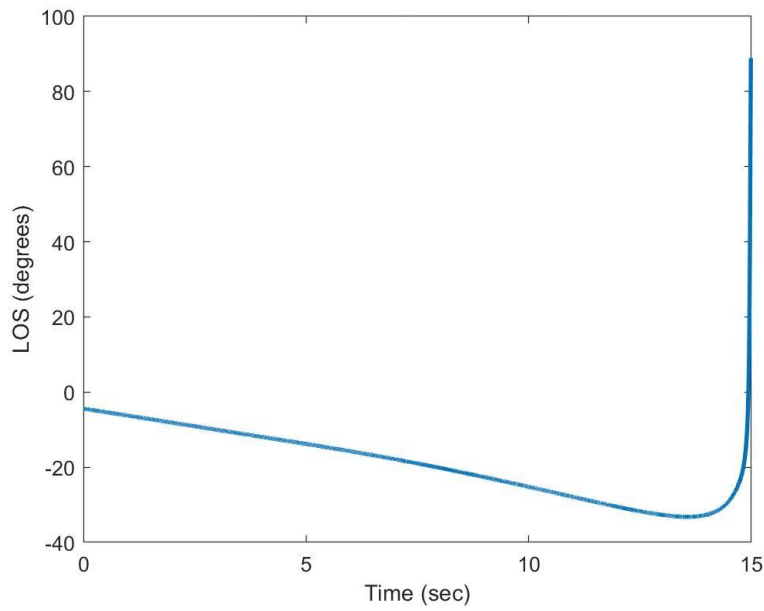
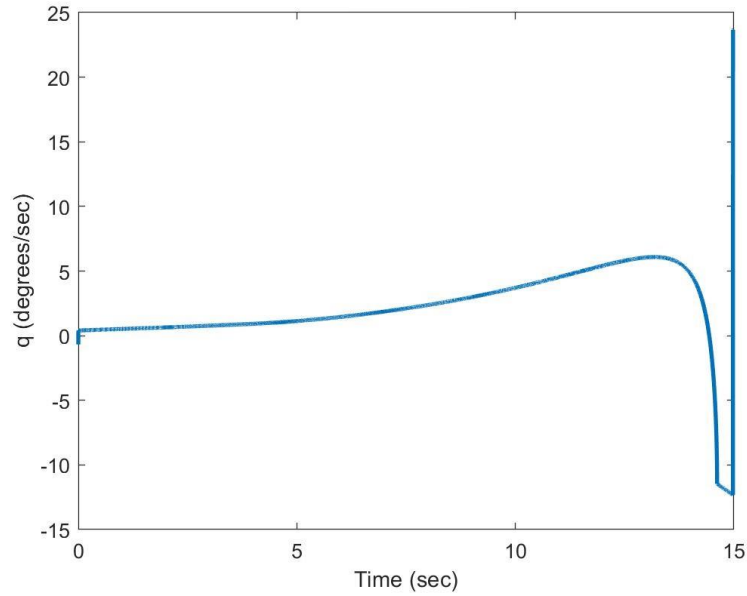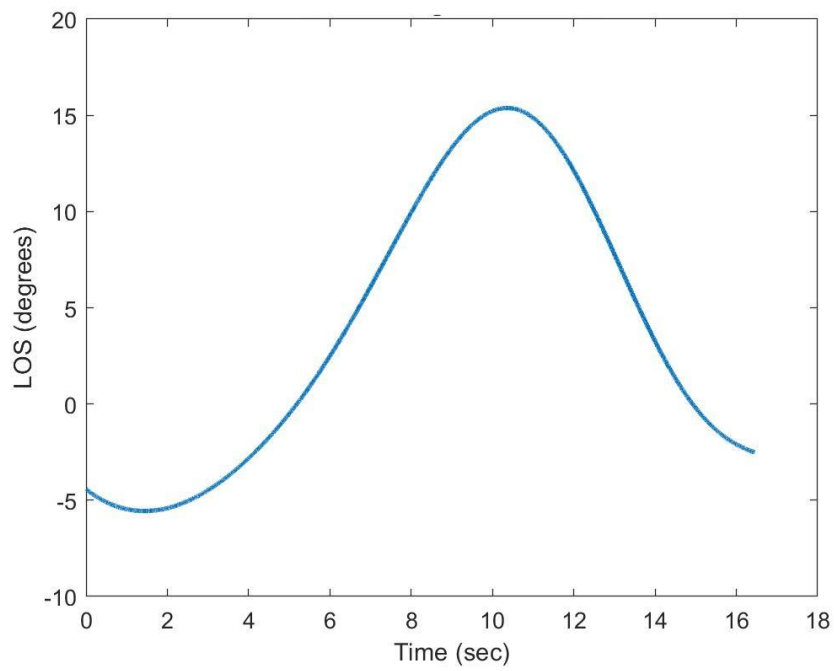Figure 19.   Line of Sight of Proportional Navigation with $N = 3$ and $k = 0.2$

Figure 20.   Control of Proportional Navigation with $N = 3$ and $k = 0.2$

When $k = 1$ the control law cannot effectively guide the missile until $N = 6$. The result can be seen in Figure 21 through Figure 23.
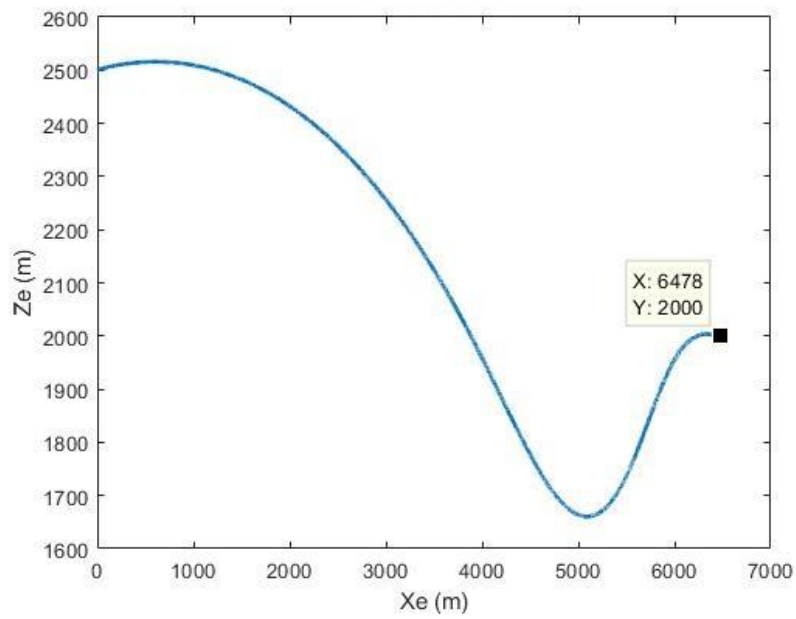
Figure 21.   Simulation of Proportional Navigation with *N* = 6 and *k* = 1

Figure 22.   Line of Sight of Proportional Navigation with *N* = 6 and *k*
= 1
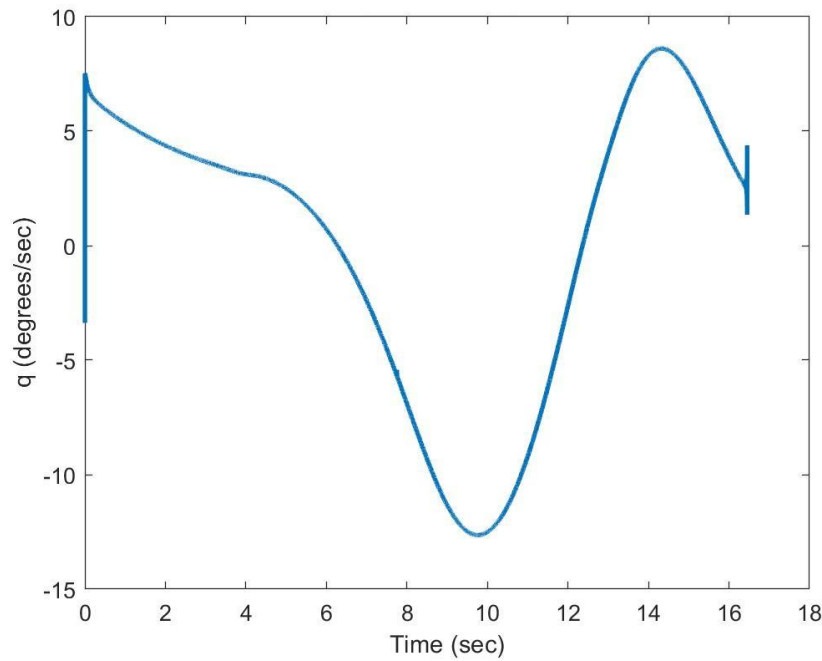
Figure 23.   Control of Proportional Navigation with $N = 6$ and $k = 1$

B.   SUMMARY

This chapter covered the derivation of the basic proportional navigation control law. The developed control law was expanded to allow the control to be useable in the high-fidelity model. The final control law was then tested by using the initial conditions of the maximum range solution and the desired position to be at the maximum range. Manipulation of the control law gains and navigation ratio was needed to ensure that the control law was able to guide the missile into the desired point. This demonstrates some of the short comings of proportional navigation. The next chapter will implement the real-time optimal control and compare its performance to rudimentary proportional navigation performance.

THIS PAGE INTENTIONALLY LEFT BLANK

VI. REAL-TIME OPTIMAL CONTROL

The maximum range solution was obtained to determine the maximum distance the missile could travel. This information was needed because it was important to ensure that the bounds for future cost functions were not asking the missile to perform beyond its capabilities, and result in an unsolvable problem. For the minimum time and maximum energy cost functions a distance of 4318m, two thirds of the maximum range, was chosen to ensure that there was enough operating room to ensure that the missile could perform the desired task.

A. MINIMUM TIME SOLUTION

The minimum time cost function was solved first in order to provide a baseline for comparing the performance of the maximum energy solution. The final time and energy from the solution are the performance parameters of interest. Figure 24 through Figure 27 provide plots of the minimum time solution, and Table 7 provides a summary of the performance.
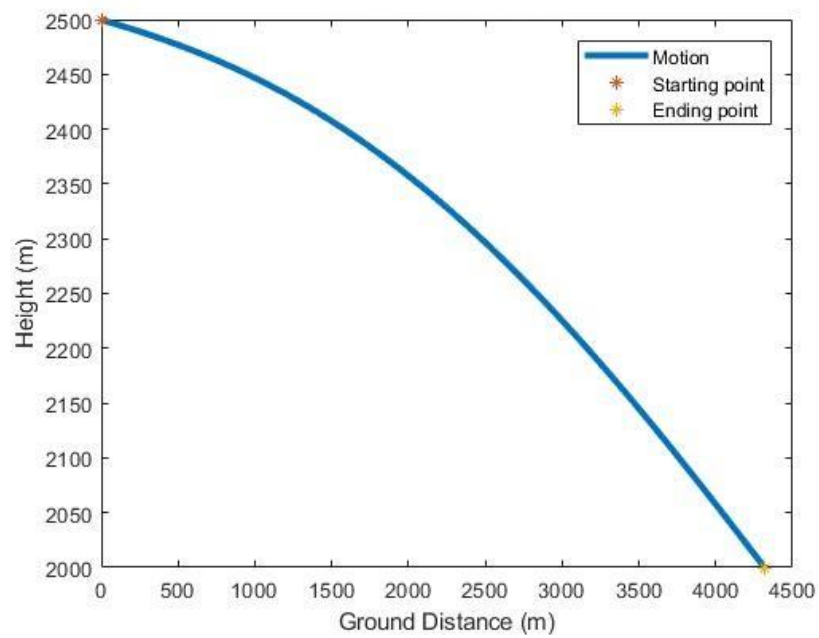
Figure 24.   Minimum Time Solution: Path
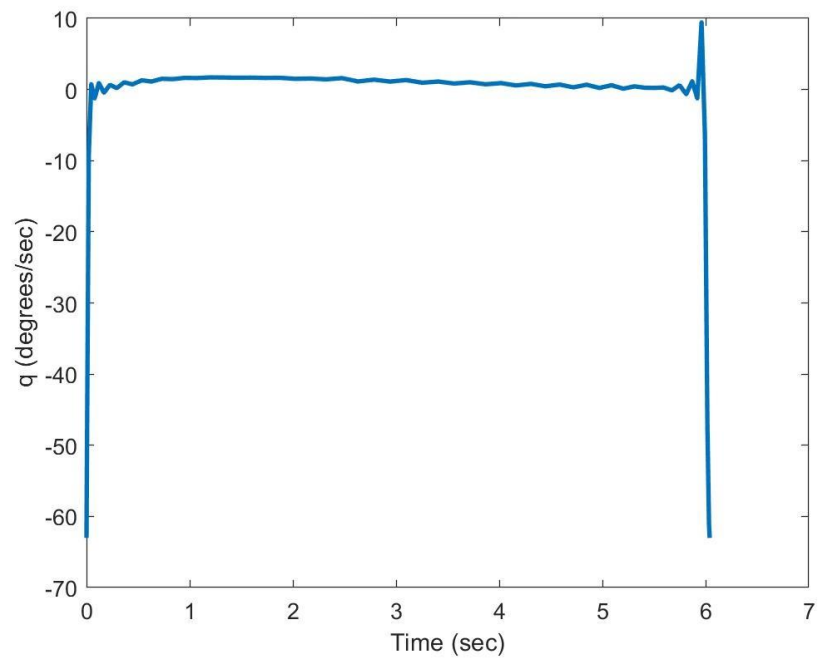

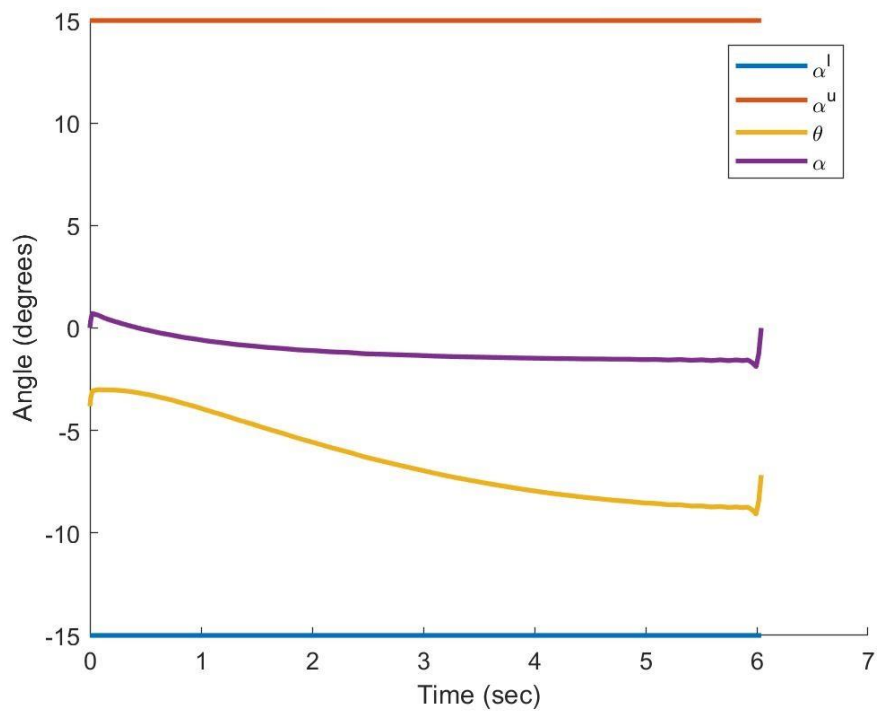Figure 25.   Minimum Time Solution: Control

Figure 26.   Minimum Time Solution: Angles
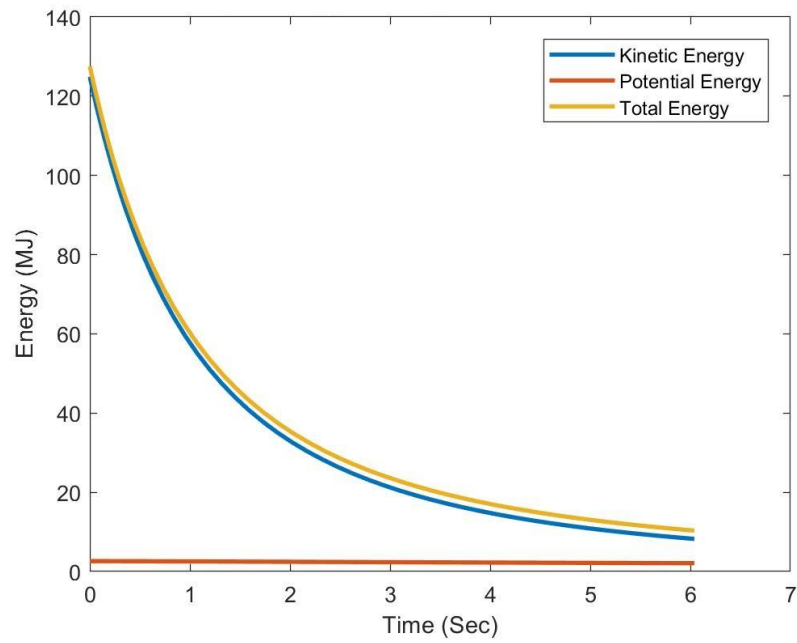

Figure 27.   Minimum Time Solution: Energy

Table 7.   Summary of Minimum Time Solution Performance

Final Time (s)	6.04
Final Kinetic Energy (MJ)	8.24

B.   MAXIMUM ENERGY SOLUTION

With the baseline obtained from the minimum time solution, the maximum energy solution is obtained. Figure 28 through Figure 31 provide plots of the maximum energy solution and Table 8 provides a summary of the performance.
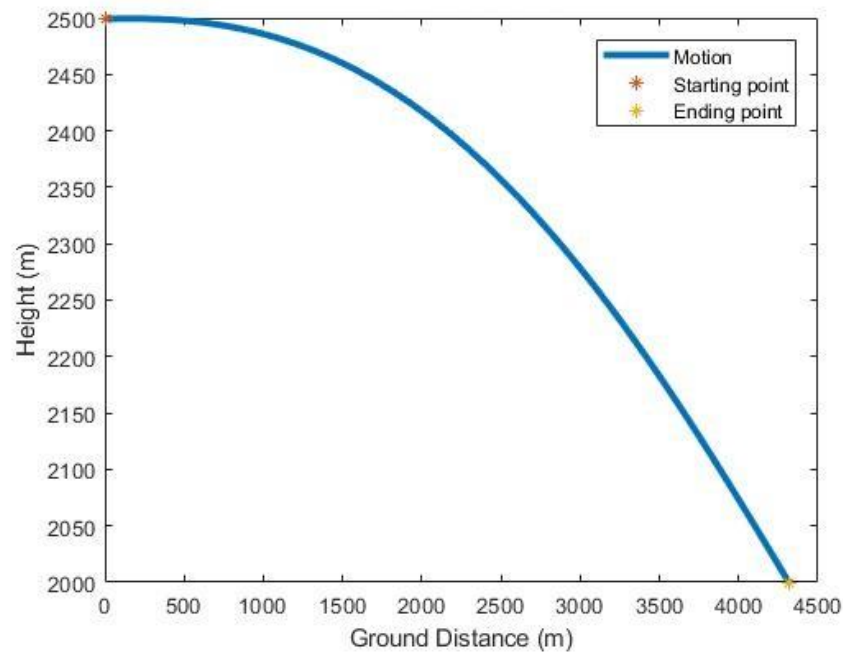

Figure 28.   Maximum Energy Solution: Path
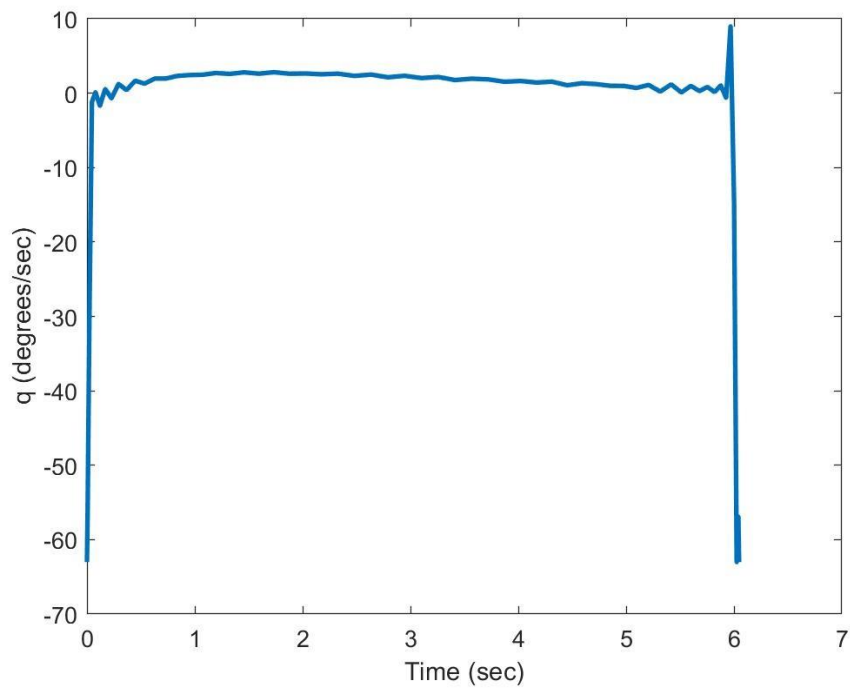
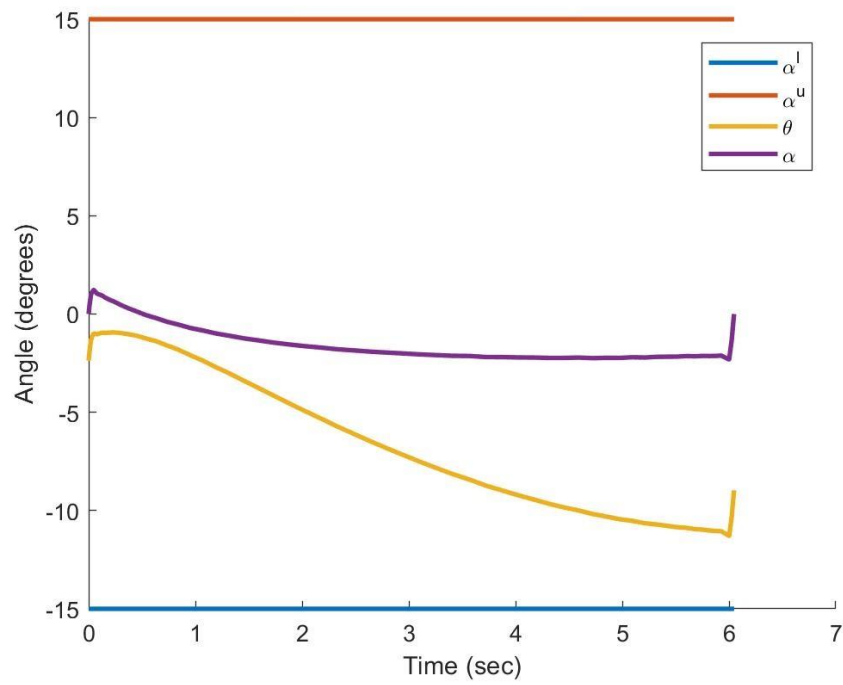Figure 29.   Maximum Energy Solution: Control

Figure 30.   Maximum Energy Solution: Angles
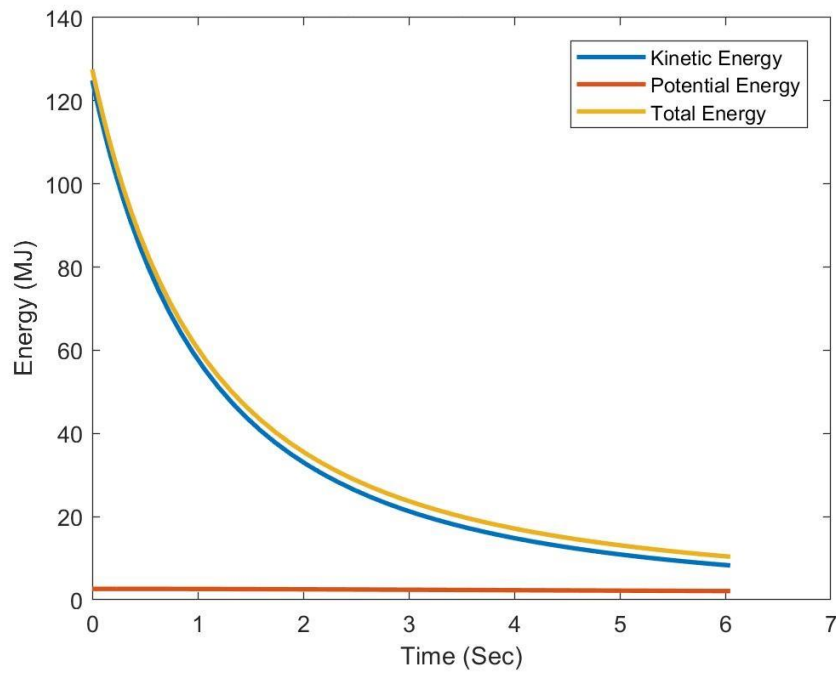
Figure 31.   Maximum Energy Solution: Energy

Table 8.   Summary of Maximum Energy Performance

Final Time (s)	6.05
Final Kinetic Energy (MJ)	8.26

Immediately when looking at Figure 24 and Figure 28, it can be seen that the results are not that dissimilar. Comparing the optimal controls, as seen in Figure 32, they nearly identical.
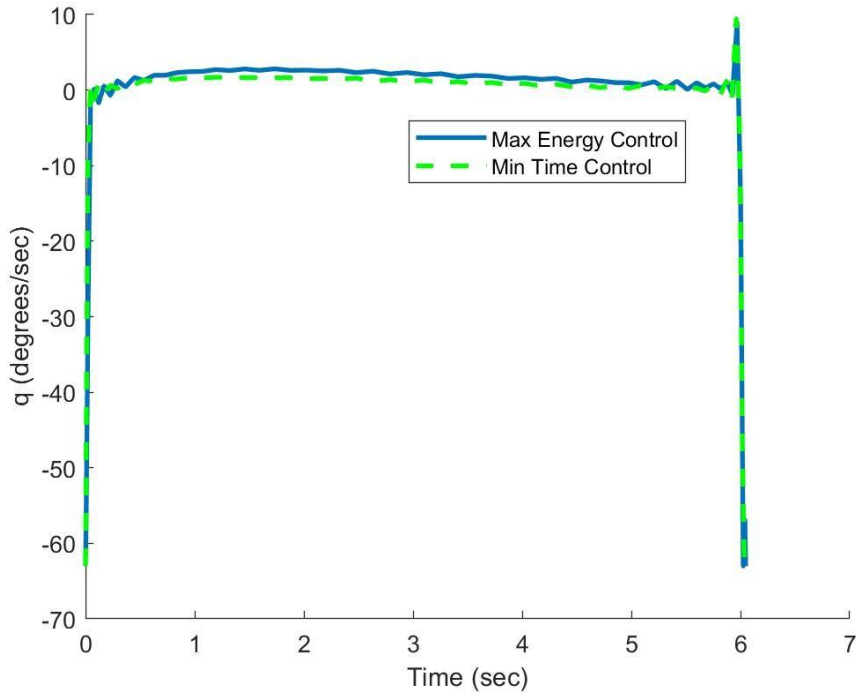
Figure 32.　　　Comparison of Maximum Energy and Minimum Time
Optimal Control

Looking at the performance of the minimum time and maximum energy solutions, their final times and kinetic energy are less than 0.3% different from each other, the two solutions are equivalent. This may be a result of the axial coefficient, *CA*, being held at a constant for the low-fidelity model.

C.　　REAL-TIME OPTIMAL CONTROL

With the maximum energy solution obtained, the optimal control, from the low-fidelity model, is then simulated using the high-fidelity model. To establish a baseline of comparison, an open loop run is conducted employing the control history obtained from the low fidelity model. Before the simulation is performed, it is important to note that the final time is expected to be greater than the solution and the final kinetic energy is expected to be less. This is because of the difference between the low-fidelity and high-fidelity models, mainly the axial drag coefficient (*CA*). *CA* was held at a constant in the

low-fidelity model, but was allowed to change in the high-fidelity model. The results of the open loop can be seen in Figure 33.
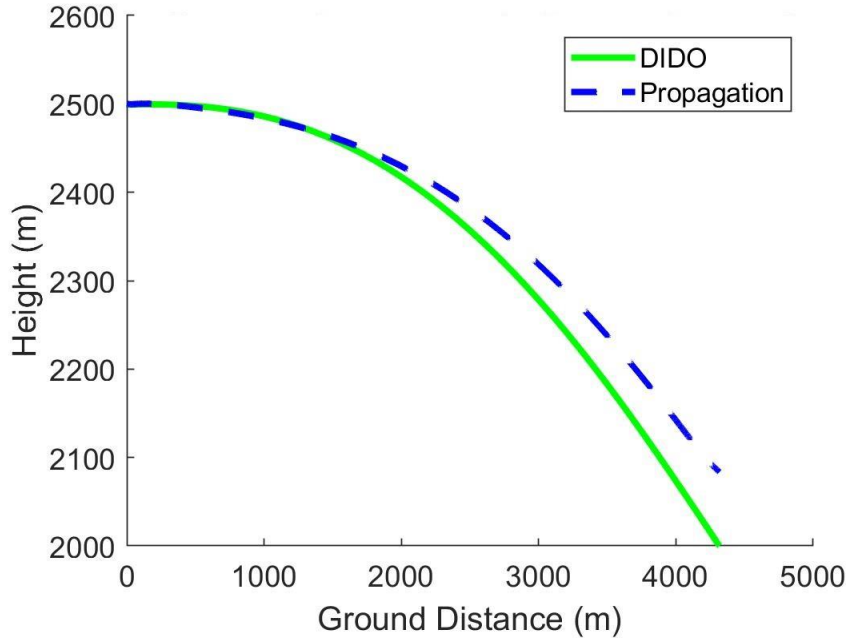

Figure 33.   Open Loop Propagation Using the Optimal Solution: Path

As it can be seen in Figure 33, the high-fidelity model is unable to follow the desired trajectory in the open loop. The propagation misses the target by about 83 m. In addition, as mentioned earlier, the final time ended up being 6.316 seconds while the final kinetic energy was 6.12 MJ.

With the baseline obtained from the open loop propagation, testing the RTOC is the next phase. The RTOC is implemented by allowing the model to be initially simulated using the optimal solution obtained from the maximum energy problem. However, the model is only allowed to propagate for a fraction of the total time of the maximum energy solution. The amount of time that the model is allowed to propagate here is known as the step time. When the propagation completes, the final states of the model are used as initial conditions to resolve the maximum energy problem. The propagation of the model then continues from its last point using the new optimal control

solution. The process is repeated a set amount of times. Once the last optimal solution is obtained, the RTOC enters what is known as "blind time" where the model must trust that final solution will guide the missile the rest of the way in.

Various step times were chosen by taking the total time from the maximum energy optimal solution and breaking it into even segments. The results from the different steps times can be seen in Table 9.

Table 9.   Summary of RTOC Performance for Various Step Sizes

Segments	Step Time (s)	Final Time (s)	Final Energy (MJ)	Miss Distance (m)
5	1.21	6.4	6.1	12.39
10	0.61	6.4	6.1	3.52
15	0.40	6.4	6.1	1.54
20	0.30	6.4	6.1	1.42
25	0.24	6.4	6.1	1.62
30	0.20	6.4	6.1	0.94

One thing to note is that increasing the numbers of steps used in by RTOC does not appear to have a significant impact on the final energy. This is most likely a result of the missile not deviating from the optimal path significantly during its initial propagation with the high-fidelity model.

Figure 34 and Figure 35 show RTOC implemented with a time step of 0.30 seconds. They demonstrate how the missile can easily follow the optimal solution with the aid of RTOC. We can see from Figure 36 the system compensates for the discrepancies in the models. Table 10 then summarizes the RTOC and open loop performances.
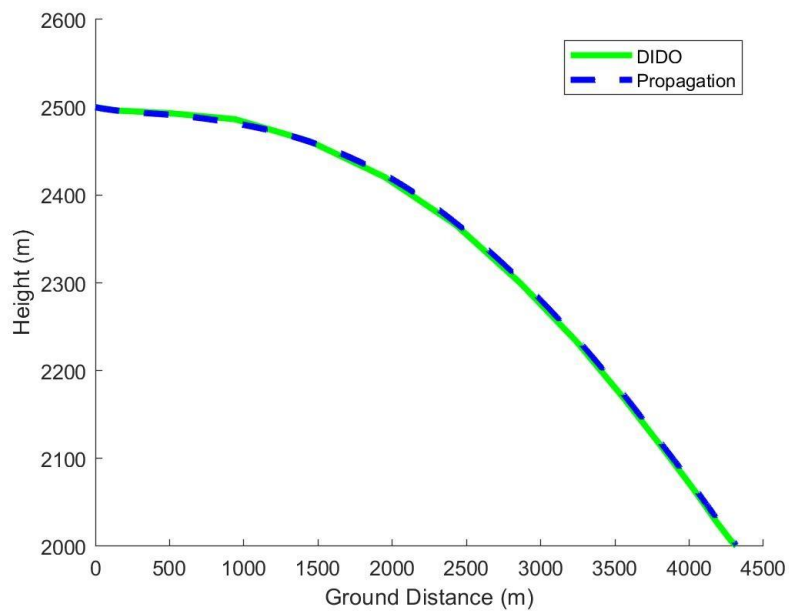
Figure 34.   RTOC Propagation Using Optimal Solution: Path
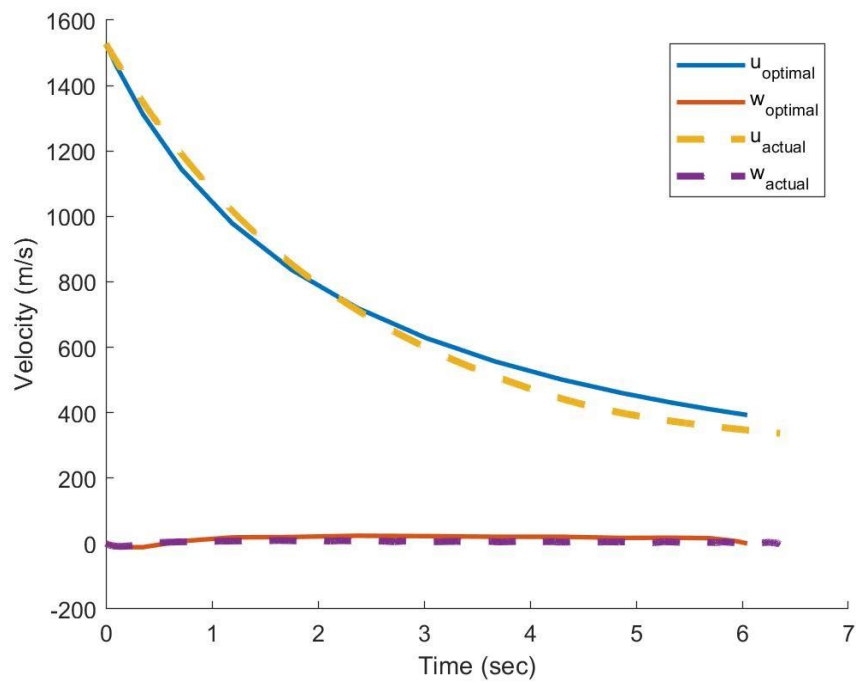

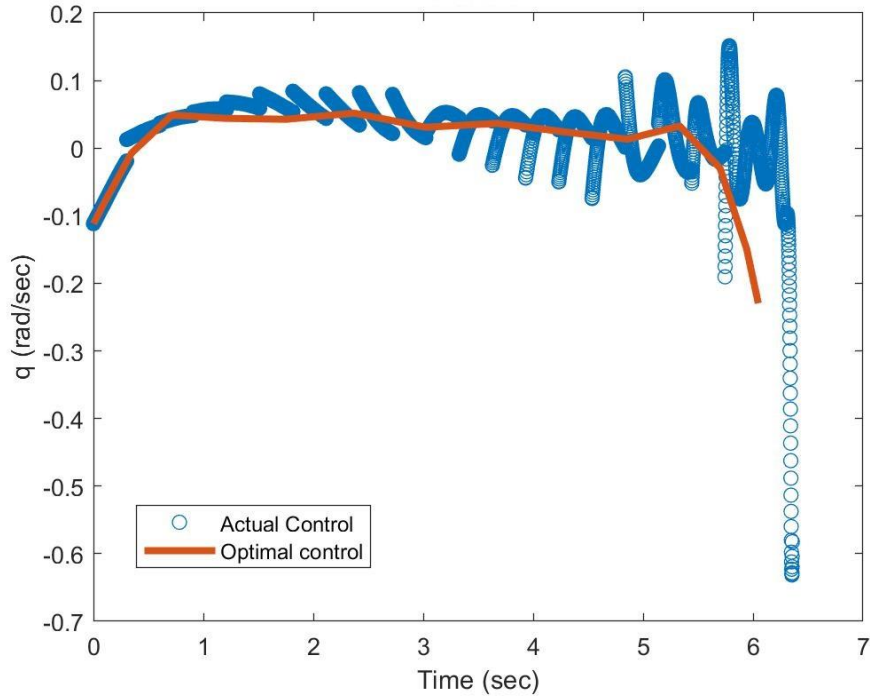Figure 35.   RTOC Propagation Using Optimal Solution: Velocity

Figure 36.   RTOC Propagation Using the Optimal Solution: Control

Table 10.   Summary of Propagation Performance

	Final Time (sec)	Final Kinetic Energy (MJ)	Miss Distance (m)
Optimal Solution	6.0	8.3	N/A
Open-Loop	6.3	6.1	83.2
RTOC: $\Delta t = 0.302$	6.4	6.1	1.4

Referring to Table 10 we can see that the RTOC method reduces the miss distance to almost 1/60th of the open loop distance, while only sacrificing less than 1% of the final kinetic energy.

As mentioned in chapter V, a proportional navigation control was implemented as an alternative method for comparison purposes. Figure 37 shows the trajectory that the

proportional navigation and the RTOC took and how they compare. Table 11 then compares the resulting times and kinetic energies.
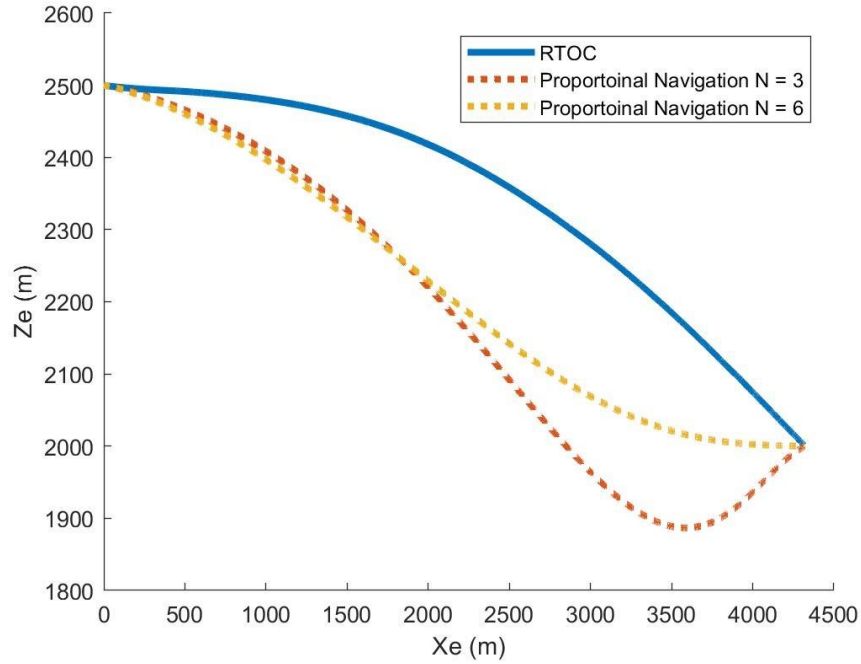

Figure 37.   Plot of RTOC and Proportional Navigation Performance

Table 11.   Comparison of RTOC and Proportional Navigation

	Final Time (sec)	Final Kinetic Energy (MJ)	Miss Distance (m)
RTOC: $\Delta t = 0.302$	6.4	6.1	1.42
Proportional Navigation (N3)	6.6	5.4	0
Proportional Navigation (N6)	6.4	5.81	0

D.   SUMMARY

In this chapter the minimum time and maximum energy optimal solutions were obtained using a reduced range obtained from the maximum range optimal solution. The

optimal solution for the minimum time and maximum energy problems were found to be equivalent, possibly due to the constant *CA*. An open loop propagation of the maximum energy problem was then obtained as a baseline for comparing the performance of the RTOC. The RTOC was then performed using different time steps to compare the impact on performance by allowing the optimal solution to be computed more often. Finally, with a time of 0.30 seconds, the results were then compared to the proportional navigation control law for a navigation ratio of three and six.

THIS PAGE INTENTIONALLY LEFT BLANK

VII. CONCLUSIONS

This thesis set out to demonstrate an alternative method for developing the control of a tactical missile with the intent on improving the conservation of kinetic energy throughout the mid-course flight. The dynamics for the three degree of freedom (3DOF) model used was first established in chapter II. After deriving the dynamics, chapter III set out to provide a means of estimating the aerodynamic coefficients of a missile when aerodynamic data is not readily available. Chapter IV then introduced the concept of optimal control theory and, as an example, went through the process of applying it the maximum range problem. Chapter IV then discussed the concepts of scaling and balancing for proper use DIDO in solving a boundary value problem. The basic proportional navigation control law and how it was applied to 3DOF model was then introduced in chapter V. Chapter VI then applied real-time optimal control (RTOC) feedback loop to the maximum energy problem to compare against proportional navigation.

The first takeaway of this thesis is that it is theoretically possible to use RTOC to guide a missile to a desired point while using only a low-fidelity dynamics model to calculate the optimal control. The RTOC was also able to accomplish this using a relatively low update rate (approximately 3 Hz).

The next major takeaway is the performance comparison of RTOC with the proportional navigation control law: RTOC had superior performance in terms of final flight time and kinetic energy compared to the standard proportional navigation. RTOC was showed to conserve more energy, $4.5\% - 12.6\%$. However, this comparison does not consider current proportional navigation methods such as gain scheduling or machine learning that could potential close performance gap.

The optimal solution derived from Pontryagin's principle on optimal control ultimately depends on the accuracy of the dynamics used to derive the boundary value problem. Any difference between the optimal control model and the behavior of the real system could potentially have a significant impact on performance of the control when

73

applied to the higher-fidelity model. In the end, though, it can be said that the RTOC method does show that it is more than capable of solving the tactical missile control problem.

Future work on investigating the potentials for the RTOC method would include using higher-fidelity models to develop the boundary value problems. One such method would be to develop best fit curves to represent the aerodynamic coefficients. Another area would be to employ fin deflection, δ, as the control input. This level of control would go beyond that which proportional navigation is capable of, and the degree of model fidelity required for practical problems could be established. In addition, more research should be conducted on using RTOC to guide a tactical missile against a moving target.

LIST OF REFERENCES

[1] M. W. Fossier, "The Development of Radar Homing Missiles*," Journal of Guidance, Controls, and Dynamics,* vol. 7, pp.641-651, November, 1984

[2] S. N. Balakrishnan, A. Tsourdos, and B. A. White, *Advances in Missile Guidance, Control, and Estimation.* Boca Raton, FL, USA: Taylor & Francis Group, 2013.

[3] K. P. Bollino, "High-Fidelity Real-Time Trajectory Optimization for Reusable Launch Vehicles," Ph.D. dissertation, Dept. of Mech. and Astro. Eng., NPS, Monterey, CA USA, 2006.

[4] U.S. Standard Atmosphere, NASA-TM-X-74335, 1976. [Online]. Available: https://ntrs.nasa.gov/archive/nasa/casi.ntrs.nasa.gov/19770009539_
1977009539.pdf

[5] P. Zarchan, *Tactical and Strategic Missile Guidance,* 4th. ed. Reston, VA, USA: AIAA, 2002.

[6] W. Blake, C. Roseman, J. Doyle, L. Auman, M. Underwood, "MISSILE DATCOM: User's manual," Wright Patterson Air Force Base, OH, 2011.

[7] A. Parsch, "Raytheon (Hughes) AIM-120 AMRAAM," Designation-Systems.Net, June 24, 2009. [Online]. Available: http://www.designation-systems.net/dusrm/m-120.html.

[8] "ENVI," Harris Geospatial Solutions, Accessed December 12, 2017. [Online]. Available: http://www.harrisgeospatial.com/softwareTechnology/ENVI.aspx

[9] T. Tyrell, C. Funk, and N. Marton, "AIM-120C-5 performance assessment for digital combat simulation enhancement," 2014. [Online]. Available: https://zaretto.com/sites/zaretto.com/files/missile-aerodynamic-data/AIM120C5-Performance-Assessment-rev2.pdf

[10] I. M. Ross, "Pontryagin's Principle," in *A Primer on Pontryagin's Principle in Optimal Control*, 2nd Ed. San Francisco, CA, USA: Collegiate Publishers, 2015.

[11] NASA Content Administrator, "NASA - F-18 Performance / Specifications," NASA, September 17, 2008. [Online]. Available: https://www.nasa.gov/centers/armstrong/aircraft/F-18/performance.html

THIS PAGE INTENTIONALLY LEFT BLANK

INITIAL DISTRIBUTION LIST

1.   Defense Technical Information Center
        Ft. Belvoir, Virginia

2.   Dudley Knox Library
        Naval Postgraduate School
        Monterey, California